Title: Physical controls on phytoplankton size structure, photophysiology and suspended particles in a Norwegian biological hotspot.

Glaucia M. Fragoso*[1], Emlyn J. Davies[2], Ingrid Ellingsen[2], Matilde S. Chauton[2], Trygve Fossum[3,4], Martin Ludvigsen[3,4,5], Kristine B. Steinhovden[2], Kanna Rajan[3,6,7], Geir Johnsen[1,3,5]

1. Trondheim Biological Station, Department of Biology, Norwegian University of Science and Technology (NTNU), Trondheim, Norway. 2. SINTEF Ocean, Environmental Technology, 7465, Trondheim, Norway. 3. Centre of Autonomous Marine Operations and Systems (AMOS), NTNU, Trondheim, Norway. 4. Department of Marine Technology, NTNU. 5. University Centre in Svalbard (UNIS), Longyearbyen, Norway. 6. Underwater Systems and Technology Laboratory, University of Porto, Portugal. 7. Department of Engineering Cybernetics, NTNU.

*Corresponding author e-mail: (Glaucia Fragoso, glaucia.m.fragoso@ntnu.no)

Present address: Trondheim Biological Station, Department of Biology, Norwegian University of Science and Technology (NTNU), Bynesveien 46, 7018, Trondheim, Norway

Keywords – phytoplankton size structure; suspended particles; *in-situ* imaging; photophysiology; automated underwater vehicles.

**manuscript is in American English

Abstract

The impact of the physical environment and phytoplankton size on particle types (zooplankton, biogenic matter or phytodetritus) in the water column is poorly understood. Here, we investigate how hydrography (e.g. water column stratification) impacts phytoplankton size and photophysiology across a productive coastal bank area. Additionally, we investigate how the physical environment and phytoplankton size structure influence the concentrations of plankton (e.g. copepods and diatom chains), biogenic forms (fecal pellets) and other particles (minerals, aggregates or phytodetritus) using discrete samples and *in-situ* optical instruments. Microphytoplankton (> 20 µm), including many chain-forming diatoms, dominated (average > 90 % of total size fraction) in un-stratified waters of the bank. Phytoplankton within the bank region also required more irradiance to saturate photosynthesis, as indicated by the onset light saturation parameter (E_k, average 297 µmol photons m^{-2} s^{-1}), suggesting high plasticity to a dynamic light environment. Conversely, the contribution of nano- and picophytoplankton (< 20 µm), such as flagellates increased (up to 36% of total phytoplankton size fraction) towards stratified off-bank waters. The phytoplankton community from off-bank had lower E_k (average 199 µmol photons m^{-2} s^{-1}) and presented higher concentrations of photoprotective pigments, such diatoxanthin - used in the xanthophyll cycle to cope with light stress and potential photo-damage. Higher concentrations of copepods (> 1×10^3 counts m^{-3}), fecal pellets (> 1×10^4 counts m^{-3}) and ammonium (> 0.5 µM) within the bank compared to off-bank regions, indicated that copepods were actively grazing in this region. Low stratification (average stratification index (SI) < 6×10^{-3} kg m^{-4}) allowed for intensive mixing, which might have promoted the high concentration of aggregates (> 5×10^5 counts m^{-3}) within the bank when compared to off-bank (SI off-bank > 10×10^{-3} kg m^{-4}). Our results, obtained using automated techniques

measured *in-situ*, represent an innovative approach to demonstrate that phytoplankton size and stratification influence the nature of particles found in the water column (including aggregates, fecal pellets and grazer abundances).

1. Introduction

The size structure and morphology of a plankton community is largely controlled by environmental factors, such as nutrient concentrations and turbulence in marine ecosystems (Acevedo-Trejos et al., 2013; Margalef, 1978). Consequently, phytoplankton size structure significantly impacts the energy transfer to upper trophic levels (Maury et al., 2007), in addition to the flux of particles to deep waters (Guidi et al., 2009; Mouw et al., 2016). For example, microphytoplankton (> 20 µm), mainly diatoms, which are common in upwelling nutrient-rich areas, are considered the main contributor to carbon export to deep waters (Kemp et al., 2006; Tréguer et al., 2018). Conversely, pico- (< 2 µm) and nanophytoplankton (2-20 µm), such as some cyanobacteria and small flagellates, dominate in stable and oligotrophic regions, and are rapidly remineralized in the upper water column (Kiørboe, 1993; Marañón, 2009). Phytoplankton size structure can also influence photophysiological parameters within a community, such as photosynthetic rates, chlorophyll *a* absorption cross-section and intracellular pigmentation (Lehmuskero et al., 2018; Uitz et al., 2008). However, the photoacclimation response of a phytoplankton community to light has been shown to be related to the amount of ambient light and depth rather than phytoplankton size structure (Bouman et al., 2018).

Many efforts have been made over the last decades to investigate the influence of marine phytoplankton on vertical flux of carbon to deep waters using sediment traps (Boyd et

al., 2005; Salter et al., 2007), marine snow catchers (Cavan et al., 2015) and *in-situ* imaging techniques (Möller et al., 2012). However, the impact of marine phytoplankton communities and size structure on the nature of particles found in the water column (from individual cells to aggregates and/or carbon intake and repackaging, e.g. fecal pellets and grazer abundances), as well as their identification and quantification, remains a challenge. That is because of the complexity of marine suspended particles, which vary in form, size, and origin: from terrestrially-derived mineral grains, plankton and bacteria, biological detritus to a mixture of all these components. Moreover, phytoplankton size, morphology and taxonomy can influence the abundance and the properties of those particles, given that phytoplankton can enhance flocculation of marine snow (aggregates composed of a variety of plankton and detritus) during blooms (Laurenceau-Cornec et al., 2015). These particles may also break up, leading to a change in their transport behavior due to differences in size and density – and therefore particulate settling flux (Davies and Nepstad, 2017). *In-situ* monitoring (identification and quantification) of particles of distinct types (fecal pellets, aggregates, phytodetritus or living zooplankton) in the water can, thus, help us to understand the mechanisms underlying particle settling and flux.

In-situ particle recording (biogenic and non-biogenic) as well as counting and identification using imaging and machine learning analyses has been considered a promising, non-destructive technique, where particle shape and size are preserved (Davies et al., 2017; Fragoso et al., 2018; Sosik and Olson, 2007). Due to the highly variable and complex nature of particles suspended in the water column, *in-situ* imaging has proved to be essential in providing accurate information on abundance of individually classified particle types, such as marine snow, copepods and diatom chains (Hu and Davis, 2006). *In-situ* monitoring also allows a combination of several sensors that are able to capture particle size from a wide range of sizes and several orders of magnitude (Boss et al., 2015; Davies et al., 2017;

Reynolds et al., 2010). The application of machine learning techniques, utilizing deep convolutional neural networks has the potential for obtaining highly accurate and rapid classification of particle types measured *in-situ* (Davies et al., 2018; Ding et al., 2018).

Coastal environments are highly productive due to upwelling, eddies or other episodic upward pulses of nutrients that continuously stimulate phytoplankton growth (Rykaczewski and Checkley, 2008). In addition to the high concentration of phytoplankton cells and chains, the intense water column mixing found in coastal systems allows aggregates and floc formation of several sizes, shapes and densities through the collision of small particles, either of a biogenic (live organisms and detritus) or non-biogenic (sediments) nature (Cross et al., 2014; Stemmann and Boss, 2012). The dynamic and episodic nature of coastal waters, however, imposes a challenge when studying the mechanisms underlying phytoplankton dynamics and particle composition. The combination of adaptive robotic sampling, such as *in-situ* profiling autonomous underwater vehicles (AUVs), with numerical ocean models can, thus, address key drivers of productivity and environmental variability (Fossum et al., 2019; Johnsen et al., 2018; Ludvigsen et al., 2018).

In this work, we provide a synthesis of information from a novel combination of *in-situ* optical instruments, particle imaging, pigment-based phytoplankton size structure and fluorescence-based photophysiology. The goal is to: 1) investigate how distinct hydrography across a bank region affects the phytoplankton composition and photophysiological state and to 2) link the phytoplankton characteristics with particle types using an *in-situ* optical image sensor. By doing so, we aim to better understand how the physical environment shapes phytoplankton size, and consequently, the upper trophic levels (e.g. copepod abundance) and particle formation (fecal pellets and aggregates), which will fill the gaps of our knowledge regarding pelagic processes and carbon fluxes in coastal ecosystems.

2. Methods

2.1 Study area

The Froan archipelago, located off the coast of mid-Norway, is considered a biological hotspot because of irregular bathymetry, where wind and tidal mixing sustain the primary productivity and biological diversity (Sætre, 2007). The area is known to be highly productive regarding seafood and fishing industry (e.g. Atlantic cod and saithe, large scallop (*Pecten maximus*) and edible crab (*Cancer pagurus*)), which boost the regional economy (Ervik et al., 2018; Julshamn et al., 2008; Tiller et al., 2015). Moreover, the Froan archipelago has a high biodiversity of fauna, being a breeding ground for the European shag (*Phalacrocorax aristotelis*) (Barrett et al., 1990), the great cormorant (*Phalacrocorax carbo*) (Lorentsen et al., 2010) and the gray seal (*Halichoerus grypus*) (Jenssen et al., 2010). Despite being an important ecological zone, little is known regarding plankton/particle distributions and dynamics in this region.

This study area of Mausund Bank (63.8°- 64.2°N, 8.2° - 9.0° E) in the Froan archipelago is a shallow bank with small islands and complex bathymetry (Fig. 1). The circulation around Froan is dominated primarily by hydrographical forcing. The main oceanic current is the Norwegian Coastal Current (NCC), which is a surface water-mass originating in the south (in the Skagerrak Strait) that mixes with freshwater runoff from Norwegian fjords as it moves northwards along the coast (Skagseth et al., 2011). Another oceanic current found in the Mausund Bank is the North Atlantic Current (NAC), which flows underneath the NCC and occasionally intrudes into the bank, bringing warm, saline and nutrient-rich waters into this area. The steep continental shelf and the complex bathymetry in the shallow Mausund

Bank provide the physical setting for upwelling events, which are fueled by strong local tidal currents (Moe et al., 2003) and wind-driven mixing in the summer (Sætre, 2007).

2.2 Sampling

Samples for nutrient and biological analyses were collected between 8th to 12th May 2017 at five different stations at Mausund Bank on board of the *R/V Gunnerus* (Fig. 1). The stations covered the area within the bank (St. 1 and 2) and off-bank area (St. 3, 4 and 5) (Fig. 1). Stations were sampled several times within the course of the five days and under distinct tidal conditions (Table 1).

A CTD (Sealogger 25, Seabird Electronics, Inc., USA) was deployed on a rosette with vertical profiles from the surface down to 100 - 250 m at each station. The Stratification Index (SI) was calculated as the absolute value of the difference in potential density (σ_Θ) between the deepest to the shallowest depth ($\sigma_{\Theta deep} - \sigma_{\Theta shallow}$) divided by the respective difference in depth ($z_{deep} - z_{shallow}$) as described in Li, 2002.

2.3 Imaging sampling

An additional profiling frame was also deployed in the upper 100 m of the water column to obtain information on optical and particle properties. Particle properties were obtained by the Silhouette Camera (SilCam) system (Davies et al., 2017). This instrument provides *in-situ* information on the particle size distribution and concentration spanning 50µm - ~11 mm in diameter. *In-situ* measurements of particulate material are necessary because marine snow flocs and other delicate particles are easily broken during discrete water

sampling. Images from the SilCam system can also be analyzed to extract information on the abundance of varying types of material present, such as diatom chains, fecal pellets and flocs (examples of images are found in Figure 2). The profiling frame was lowered at approximately 0.2-0.4cm/s, with data acquisition rates for the CTD at 1Hz and the SilCam at 7Hz.

The SilCam is an *in-situ* particle imaging system that utilizes telecentric receiving optics, a white backlight and a high-resolution color camera to record transmittance images (Davies et al 2017). The sample volume of the system used here was 35.2 x 29.4 x 11mm for each raw image recorded. *In-focus* particle images are directly recorded in color, so minimal processing is needed. These images look very much like microscope images (albeit at a lower magnification). From raw images, individually-detected particles are counted, sized and classified with a minimum equivalent circular diameter of 50 µm (corresponding to a 12 pixel area).

2.4 L-AUV sampling

The Light Autonomous Underwater Vehicle (L-AUV, Sousa et al., 2012) was equipped with a Seabird Fastcat 49 CTD (sampling rate of 16 Hz) for temperature, salinity (conductivity) and depth (pressure) parameters. A Wet Labs Eco Puck (Wet Labs, Oregon, USA, calibrated by producer prior to cruise) was also equipped on the L-AUV for fluorescence detection of chlorophyll *a* (Chl$a_{\text{in-situ}}$, in mg m^{-3}) and colored dissolved organic matter concentrations (CDOM, in ppm). The concentration of total suspended material (TSM) was detected by back scattered light at 700 nm (b_b700, m^{-1}). Two transects were performed, one on the 8th May for 3 hours (10:30 am – 1:30 pm) back and forth in the region within the bank (transect A, Fig. 1) and another one off-bank (transect B) on the 5th May for 4

hours (2:30 pm – 16:30 pm). More details about the adaptive sampling strategy with the L-AUV is available in Fossum et al. (2018).

2.5 Water and net sampling

Water samples were collected from 2.5 L Niskin bottles mounted on the CTD rosette frame. Discrete water samples were collected at the surface (< 5 m) and subsurface (25 and 40 m) for measurements of phytoplankton pigments (including *in vitro* chlorophyll *a* as an indicator of phytoplankton biomass), and *in vivo* variable chlorophyll *a* fluorescence (Phyto-PAM) for photosynthetic parameters. At stations 3, 4 and 5, which were more stratified, samples were also collected at deeper waters for nutrients (80 to 120 m). Net hauls were sampled at the surface (< 5 m) for analysis of phytoplankton communities, using a plankton net (mesh size 20μm) and fixed with formaldehyde to a final concentration of 4%. The fixed samples from net hauls were kept in the dark at room temperature for later identification.

Samples for nutrients were filtered with a 0.8 μm polycarbonate filter and the filtrate was placed in a centrifuge tube and frozen at -20ºC. Nutrients concentrations (nitrate+nitrite, silicate, phosphate and ammonium) were analyzed later using a continuous flow automated analyzer (CFA, Auto Analyzer 3, SEAL).

For pigment analyses (chlorophylls and carotenoids), water was filtered (0.5 L – 2L, depending on biomass) onto a Whatman GF/F glassfiber filter and on-board of the *R/V Gunnerus*. Filtration volumes were adjusted based on how much biomass was concentrated in each filter. After filtration, each filter was double-folded, wrapped in aluminum foil, immediately flash-frozen in liquid nitrogen and kept temporarily (during the cruise) in a liquid nitrogen shipper. After the cruise, samples were immediately transferred and stored in a -80ºC

freezer until analyses in the laboratory to minimize pigment degradation (Johnsen and Sakshaug, 1993).

2.6 Image processing

Classification of particles (copepod, diatom chain, fecal pellets, etc.) is obtained via a Deep Convolutional Neural Network implemented with Tensorflow (Abadi et al., 2016). The analysis of SilCam data is performed using PySilCam (github.com/emlynjdavies/PySilCam), which uses the workflow described by Davies et al., (2018). The following main processing steps are applied to each image recorded by the SilCam:

1. Each image is corrected by a clean background image to reduce noise.
2. The corrected image is segmented (binarized) to produce a logical image (zeros and ones) of the particles detected.
3. Particles in the binary image are then counted and particle properties (geometry and particle type) are calculated for each particle.
4. The particle size distribution is calculated by counting Equivalent Circular Diameters (ECD) into their appropriate volume size class.
5. Particle volume is estimated by assuming the spherical volume-equivalence of the ECD.

The background correction is calculated from an average of images recorded immediately prior to processing. The correction of images reduces noise and gradients in background illumination and small fouling artefacts that may appear on the optical window. To confirm accuracy of the particle sizes in the water, validation was performed using spherical standards as reported in Davies et al. (2017).

2.7 Pigment analyses

Chlorophyll *a* concentration was determined by fluorometry (Chla_{Fluor}) and high-performance liquid chromatography (HPLC) (Chla_{HPLC}) 4 months after collection. Chla_{Fluor} was measured first through extraction in 100% methanol after 2 hours at -10°C, and determination using the non-acidification method (Holm-Hansen and Riemann, 1978) and a Turner Designs Trilogy fluorometer (model: 7200-000). Furthermore, individual chlorophylls and accessory pigments were quantified using a reverse-phase HPLC (Hewlett-Packard 1100 Series system) equipped with a diode array detector (spectral absorbance), where pigments were separated using a Symmetry C8 column. The method is described in Rodríguez et al. (2006) with modification from Zapata et al. (2000), and referred to as 'HPLC system 2' in Egeland et al. (2011). Frozen filters were extracted with 100% methanol for at least 24 hours at -20ºC. Extracts were filtered through Millipore 0.45 µm filter syringe to remove debris before injection into the HPLC system. HPLC calibration was performed using chlorophyll and carotenoid standards from own cultures and from SIGMA (Aldrich, UK) and DHI Water & Environment (Denmark). Specific extinction coefficients used for pigment quantification were found in Jeffrey et al. (1997). Limits of detection were 0.001 mg m^{-3} for all pigments and pigment concentrations below detection limits were not reported.

2.8 Phytoplankton size structure determination

Many phytoplankton species typically found in coastal regions (e.g. the diatom *Skeletonema*) are sensitive to chlorophyllase activity, which results in the degradation of Chla_{HPLC} to chlorophyllide *a* and pheophorbide (sub-products of Chla_{HPLC}) (Barrett and

Jeffrey, 1971; Jeffrey and Hallegraeff, 1987; Roy et al., 1996; Suzuki and Fujita, 1986). Chlorophyllase activity has been assumed to increase in aqueous solvents, such as those used in HPLC analysis (Barrett and Jeffrey, 1971, Jeffrey and Hallegraeff, 1987) or during the breakage of weakly silicified cells walls (typically found in *Skeletonema*) and chloroplast damage, which releases the acidic cell sap (Roy et al., 1996; Johnsen and Sakshaug, 1993; Suzuki and Fujita, 1986).

In this study, the presence of chlorophyll *a* degradation products, such as chlorophyllide *a* and phaeophorbide *a* was observed, so we infer that some degradation occurred possibly because of the dominance of *Skeletonema costatum*. *In vitro* chlorophyll *a* degradation can compromise the determination of phytoplankton groups, such as those that use a combination of pigment marker ratios to Chla_{HPLC} (e.g. CHEMTAX). Therefore, phytoplankton size structure in this study was determined based on the ratio of selected class-specific pigment markers (which excludes Chla_{HPLC}, see below) to the sum of total diagnostics pigment (DP). This approach has been widely used in oceanographic approaches (Poulton et al., 2006; Uitz et al., 2006; Vidussi et al., 2001) and provides a simplified estimation of phytoplankton size classes. The selected pigment markers were associated with taxonomic groups from the micro- (> 20 µm, e.g. diatoms and dinoflagellates), nano- (from 2 to 20 µm, e.g. mostly flagellates) or picophytoplankton classes (< 2 µm, e.g. the cyanobacteria *Prochlorococcus* and *Synechoccocus*). The quantification was according to Poulton et al. (2006), with the modification that prasinoxanthin, a photosynthetic carotenoid of some prasinophytes, was included in the sum, given that this pigment was observed in this study and this phytoplankton group is commonly found in Norwegian coastal waters (Higgins et al., 2011; Johnsen and Sakshaug, 2007; Volent et al., 2011). In spite of some degradation of Chla_{HPLC} and the presence of chlorophyllide *a* and phaeophorbide *a* in the samples in this

study, Chla_{HPLC} and DPs were correlated (r^2= 0.77, n= 28, $p < 0.001$), providing confidence in the method used (Vidussi et al., 2001).

The approach used by Poulton et al. (2006) and Vidussi et al. (2001) is more simplistic, since it gives equal weight to all DPs. Other up-to-date and refined approach (e.g. Uitz et al., 2006) provides distinct weights of DPs, with the intention to more accurately estimate chlorophyll *a* concentrations associated with each size class. In this study, a more simplistic (former) approach was used, since the ultimate goal is to observe general spatial trends of phytoplankton size based on approximations rather than quantifying each class fraction in terms of chlorophyll *a*. Moreover, with this approach, Pras can be included in the calculation, given that it was not represented in the approach by Uitz et al. (2006). Regardless, estimations of phytoplankton size structure based on DPs must always be interpreted with caution because they do not reflect the true size of phytoplankton communities (Uitz et al., 2006). Several algal groups share similar pigment markers (Fuco is found in diatoms, as well as some prymnesiophytes, dinoflagellates and pelagophytes) and may present distinct size spectra (e.g. diatoms, which are generally considered part of the microphytoplankton can also be found in smaller sizes (< 20 µm)) (Uitz et al., 2006).

Zeaxanthin (Zea) is indicative of cyanobacteria, chlorophytes and prasinophytes Type 2 (Vidussi et al., 2004). In this study, Zea was observed as a trace pigment only (i.e. a peak was observed but its concentration was found below the limits of detection). For this reason, we removed Zea of the analyses. Chlorophyll *b* (Chl *b*) is a pigment marker found in prochlorophytes, chlorophytes, prasinophytes and euglenophytes (Jeffrey et al., 1997). It is more likely that Chl *b* belongs to prasinophytes, including the picoeukaryote *Micromonas pusilla*, given that this group has been observed in high abundances in Norwegian coastal waters (Volent et al., 2011). Therefore, we grouped the nano- and the picophytoplankton together (herein defined as N_f+P_f, see below) to represent the < 20 µm size fraction in the

further analyses. By doing so, we reduce any potential uncertainty related to Chl *b* being found in the two size groups. Alloxanthin (Allo) is a characteristic pigment of cryptophytes (Jeffrey and Vesk, 1997). Fucoxanthin (Fuco) is the major carotenoid found in diatoms, although it is also found in prymnesiophytes, chrysophytes, pelagophytes and dinoflagellates Type 2 (Higgins et al., 2011). Photosynthetic carotenoids, such as 19′-hexanoyloxyfucoxanthin (Hex-fuco) and 19′-butanoyloxyfucoxanthin (But-fuco) are the main markers of prymnesiophytes and pelagophytes, respectively, although they can also be found in dinoflagellates Type 2 and dictyochophyceae (Higgins et al., 2011; Johnsen et al., 2011). Peridinin (Per) is the marker restricted to dinoflagellates Type 1 (Higgins et al., 2011). Per, Fuco, Chl *b* and Hex-fuco were detected in all samples, whereas But-fuco was observed in 40% and Pras and Allo were found in 14% of samples. Although these latter two pigments were found in few samples (14%), we decided to keep in the approach, given that they are important markers of flagellates present in the water.

A total of eight pigments was summed to calculate the DPs as:

$$DPs\ (mg\ m^{-3}) = Chl\ b + Allo + Hex\text{-}fuco + But\text{-}fuco + Fuco + Per + Pras,$$

Where phytoplankton size classes are estimated as follow:

Microphytoplankton fraction (size range > 20 μm, M_f) = (Fuco + Per)/DPs

Nano- + picophytoplankton fraction (size range < 20 μm, N_f+P_f) = (Chl *b*, Allo + Hex-fuco + But-fuco + Pras)/DPs

To determine the xanthophyll de-epoxidation state (%), which infers whether the phytoplankton community is being exposed to light stress, the epoxidized (diadinoxanthin, DD) and the de-epoxidized form (diatoxanthin, DT) was calculated as DT/(DD+DT) and (DD+DT)/Chla_{Fluor} (Lavaud et al., 2004), where chlorophyll *a* is derived from fluorometry rather than HPLC analyses. The solvent used in determining Chla_{Fluor} (as opposite toChla_{HPLC}) is not aqueous (100% methanol, see section 2.7), which prevents chlorophyllase activity and, therefore, chlorophyll *a* degradation during laboratory analyses (Jeffrey and Hallegraeff, 1987).

2.9 Phytoplankton photophysiology

I*n vivo* variable chlorophyll *a* fluorescence was measured using a Pulse Amplitude Modulation fluorometer (Phyto-PAM, Heinz Walz) on board of the *R/V Gunnerus*. Water samples were dark acclimated and the temperature inside the PAM cuvette chamber was adjusted to the *in-situ* water temperature for 5 minutes prior to the determination of the effective PSII quantum yield (Φ_{PSII}, detailed in Nymark et al. 2009). Discrete measurements were performed on water samples collected from surface and subsurface waters (< 5 m and 25 m only) and pseudo-replicates (i.e. subsamples of the water collected from the same Niskin bottle) were measured at each depth.

Measurements of photosynthesis or electron transport rate (ETR, µmol electrons m^{-2} s^{-1}) versus irradiance (P vs E curves) were performed to determine the following phytoplankton photophysiological parameters: electron transport rate efficiency (α), maximum electron transport rate (ETR_{max}) and light intensity approximating the onset of saturation (E_k). The steps in irradiance levels varied from low to high irradiance (set from ~30 to 700 µmol

photons m^{-2} s^{-1}). The model for curve fitting was performed in each curve and all parameters were based on Jassby and Platt (1976) model, which assumes that photosynthesis achieves a hyperbolic tangent function and disregards photo-inhibition.

2.10 Phytoplankton composition

Sub-samples from the preserved net haul samples were analyzed using a Nikon Eclipse 50*i* light microscope, where observed species were registered to provide a list of dominating phytoplankton species (> 20 μm) during the survey period. Phytoplankton were identified to genus or species whenever possible, following Throndsen et al. (2007) and Tomas (1997).

2.11 Statistical analyses

Phytoplankton size structure in Mausund Bank was investigated using PRIMER-E (v7) software (Clarke and Warwick, 2001). Phytoplankton size fraction (% of nano- + picophytoplankton (< 20 μm) and microphytoplankton (> 20 μm) to the total) were analyzed using non-metric multi-dimensional scaling (nMDS) of samples based on Bray-Curtis similarity matrices. The nMDS plot was used to visually display the similarities of the samples, where samples with high community resemblances were located spatially closer than the less similar ones. The stress level of the nMDS plot is a measurement of visual representation, with low stress values (< 0.05) being associated with excellent visual representation of the similarity relationship in 2-D space (Clarke and Warwick, 2001).

A redundancy analysis (RDA) was performed using the CANOCO 4.5 software (CANOCO, Microcomputer Power, Ithaca, NY) to analyze the environmental variables

(explanatory variables) that best explain the distribution of the phytoplankton size fractions from Mausund Bank. The RDA generates an ordination diagram with arrows that show associations between each size group and the explanatory and supplementary variables. Arrows representing environmental (nutrients and hydrographic variables), biological (phytoplankton size structure) or supplementary variables (particle types, chlorophyll *a* and photoprotective pigments) in the same or opposite direction suggest positive or negative correlations; and the longer the arrow, the stronger the correlation. Conversely, no proximity indicates weak or a lack of correlation. Forward-selection (*a posteriori* analysis) and Monte Carlo permutation test (n=999, reduced model) was applied to test the statistical significance ($p < 0.05$) of the environmental variables that significantly explained phytoplankton size distribution analyzed either individually (λ_1, marginal effects) or together with other forward-selected variables (λa, conditional effects). Further information about the RDA analyses is found in Fragoso et al. (2016).

3. Results

3.1 Hydrography

Vertical profiles of temperature and salinity from stations 1 and 2 (within the bank, region A) and stations 3, 4 and 5 (outside of the bank, region B) suggest that these two regions are characterized by distinct hydrography (Fig. 3). In region A, the water column was well mixed, with temperature from 7.2 - 7.5 ºC from surface to deep waters (approximate 100 m, Fig. 3a). Conversely, at region B, temperature varied with depth, from < 7.3 ºC in the upper 100 m, increasing gradually from 50 to 110 m and up to 7.6 - 8.1 ºC at 200 m, indicating the influence of Atlantic water at this depth (Fig. 3a). Salinity and density (σ_Θ) had similar patterns in both regions, suggesting that stratification is mostly driven by changes in

salinity (Fig. 3b,c). In both regions, salinity and density were generally lower at the surface (region A, salinity < 34 and σ_Θ < 26.5 kg m^{-3}; region B, salinity > 34 and σ_Θ > 26.5 kg m^{-3}), increasing with depth (region A, salinity = 34.2 and σ_Θ= 26.7 kg m^{-3} in 110 m approximately; region B, salinity up to 35.2 and σ_Θ= 27.4 kg m^{-3} at 200 m) (Fig. 3b,c). The larger change in density with depth in region B (Fig. 3c) contributed to greater stratification when compared to region A as observed in the upper 100 m (maximum SI values > 0.02 kg m^{-4}, Fig 3d).

3.2 L-AUV measurements

Vertical profiles of physical and biological parameters collected by sensors (Wet Labs Eco Puck and CTD) equipped on the L-AUV are shown in Figure 4. Temperature and salinity, in addition to concentrations of Chl$a_{\text{in-situ}}$, colored dissolved organic matter (CDOM) and total suspended material (TSM, analyzed as optical backscatter, b_b700) showed distinct patterns in transects at regions A (within the bank) and B (off-bank, Fig. 4). In transect A, temperature and salinity changed slightly with depth, with warmer and fresher water at the surface (temperature ~ 7.4 ºC; salinity < 33) and cooler and more saline waters from 40 to 100 m depth (average temperature = 7.2ºC and average salinity = 34) (Fig 4b,d). Conversely, in transect B, temperature was the highest at the surface (< 10 m) and below 80 m (> 7.2 up to 7.8 ºC), whereas salinity considerable increases from the surface (< 5 m, average = 33.5) towards deeper waters (average = 35 from 80 to 100 m), indicating the presence of warm and saline waters of Atlantic origin (Fig. 4c,e). In general, Chl$a_{\text{in-situ}}$ concentration was higher in transect A than transect B, where high values (~4 mg Chl$a_{\text{in-situ}}$ m^{-3}) extended down to 40 m (Fig. 4g,f). In transect B, on the contrary, Chl$a_{\text{in-situ}}$ concentrated in the upper 20 m (~3 mg Chl$a_{\text{in-situ}}$ m^{-3}, Fig. 4g). Likewise, concentrations of CDOM and b_b700 were higher at transect A than B (Fig 4 h-k), particularly in the upper 40 m (CDOM > 2.7 ppm, b_b700 > 0.0002 m^{-1},

Fig 4i, k), suggesting that they occur as a result of high phytoplankton concentration (observed by Chl$a_{\text{in-situ}}$ values) found within bank area.

3.3 Phytoplankton size and community structure

Phytoplankton size structure varied from within the islets to outside of the bank area but not with depth (Fig. 5a). As observed in the nMDS analysis, phytoplankton at station 1 and 2 had higher similarity values among stations in terms of size structure, and was dominated by microphytoplankton (Fig. 5b, average = 91%, Table 2), particularly diatoms (see species list, Table S1, supplementary material). The contribution of the phytoplankton < 20 µm (nano- + picophytoplankton) increased while microphytoplankton decreased, from inshore (St. 1) to offshore (St. 5) (Fig. 5), reaching an average of 25% and 73% at stations 5, respectively (Table 2).

Net haul samples were dominated by diatoms and dinoflagellates. The number of listed species varied from 11 at the outmost station (St. 5), to 29 and 31 at the innermost (St. 1 and 2, respectively (Table S1, supplementary material). The dominant diatom was *Skeletonema costatum*, which was observed at all stations during the cruise. The toxic (PSP, Paralytic Shellfish Poison) dinoflagellate, *Alexandrium tamarense*, was also recorded in all samples, except at the station 5 (Table S1, supplementary material). A variety of large dinoflagellates (e.g. *Tripos* spp., *Protoperidinium depressum*) and chain-forming diatoms (e.g. *Chaetoceros* spp., *Thalassiosira gravida*) were observed (Table S1, supplementary material), which consistent with the SilCam observations. Information on nano- and picophytoplankton in the net hauls is limited due to the sampling method and fixation.

3.4 Phytoplankton photophysiology

Photosynthetic parameters obtained from *P vs E* curves differed between regions within and outside the bank. In region A, phytoplankton presented high electron transport rate (average ETR_{max} = 49 µmol electrons m^{-2} s^{-1}), indicating higher photosynthetic rate when compared to region B (average ETR_{max} = 36 µmol electrons m^{-2} s^{-1}) (Table 3). Phytoplankton from within bank region also appeared to require more irradiance to saturate photosynthesis (average E_k for station 1 = 311 µmol photons m^{-2} s^{-1}), decreasing gradually towards off-bank (average of station 5 = 190 µmol photons m^{-2} s^{-1}) (Table 3, Fig. 6). Phytoplankton from station 3 (part of region B) presented similar photophysiological traits as observed in phytoplankton from region A (St. 1 and 2), with high ETR_{max} (~ 49 µmol electrons m^{-2} s^{-1}) (Table 3, Fig. 6). Conversely, E_k did not vary at different depths (surface and 25 m, Table S2, supplementary material).

3.5 Particle distributions

Particle composition and concentrations obtained from the SilCam showed distinct patterns among stations (Fig. 7). In general, concentrations of copepods (> 1×10^3 counts m^{-3}), fecal pellets (> 1×10^4 counts m^{-3}), diatom chains (> 2×10^4 counts m^{-3}), and other particles (> 5×10^5 counts m^{-3}) were higher within St. 1 and 2 (region A) than the other stations (Fig. 7, Table 2). At this region, concentrations of particles were similar within depth, confirming a strong mixing found in this region (Fig. 7). As opposed to region A, fecal pellets, diatom chains and other particles were higher in the upper 30 m in region B, decreasing gradually with depth and approaching undetectable counts from 70 to 100 m (Fig. 7b-d).

In terms of volume per water sampled (cm^3 m^{-3}), particles identified by the SilCam varied both from inshore to offshore (from St. 1-5) and vertically (1-20 m, 21-50 m, 51-100

m) (Fig. 8). Region A (St. 1 and 2) had, on average, high volume of particles (copepods, fecal pellets and diatom chains) at all depths (Fig. 8), except at surface/subsurface (1-20 m) waters of station 4, where large volume of fecal pellets and diatoms were observed (Fig. 8a). Fecal pellets, followed by diatom chains and copepods, contributed to most of the volume of identified particles, except at upper waters of station 4 (1-20 m), where diatom chains co-dominated (Fig 8a). Particles, in terms of volume, decreased sharply at mid-depth (21-50 m) from region A (St. 1 and 2) to region B (St. 3, 4 and 5) and gradually at deeper waters (51-100 m) from inshore (St. 1) to offshore (St. 5) (Fig 8b,c).

3.6 Environmental controls on phytoplankton size structure

Environmental variables that explained the variance (explanatory variables) in the phytoplankton size structure (% of nano- +picophytoplankton and microphytoplankton) were investigated using redundancy analysis (RDA) (Fig. 9). The associations in the ordination diagram showed that the microphytoplankton fraction, which was higher at stations 1 and 2, are predicted to correlate positively with temperature (average temperature = 7.3 °C) and dissolved inorganic nitrogen concentrations, such as nitrate+nitrate and ammonium (average of NO_3+NO_2 = 2.2 μM and NH_4 = 0.65 μM, Table 2, Fig. 9). Likewise, microphytoplankton fraction correlated positively with particles derived from the SilCam estimations (supplemental variables), such as diatom chains (> 8×10^4 counts m^{-3}), copepods (> 1×10^3 counts m^{-3}), fecal pellets (> 2×10^4 counts m^{-3}) and other particles (> 1×10^6 counts m^{-3}, Fig. 9, Table 2). Conversely, nano- + picophytoplankton size fraction, which mostly occurred in stations 4 and 5, correlated positively with stratification (average SI > 1×10^2 kg m^{-4} for St. 3 and 5) and silicate (average $Si(OH)_4$ > 1.0 μM, Table 2). Ratios of photoprotective pigments

of xanthophyll cycle, such as (DD+DT)/Chla_{Fluor} and DT/(DD+DT) (supplementary variables) also correlated positively with the nano- + picophytoplankton size fraction from stations 4 and 5 (Fig. 9), where ratios were > 0.2 (Table 2).

Forward selection showed that three out of seven environmental factors (silicate, ammonium, and nitrate+nitrate) best explained the variance in the phytoplankton size fraction when analyzed together (conditional effects, referred to as λ_a in Table 4). Silicate was the most significant explanatory variable (λ_a = 0.51, p = 0.001), followed by nitrate+nitrite concentration (λ_a = 0.18, p = 0.001) (Table 4). Ammonium concentration was also a significant explanatory variable (λ_a = 0.06, p = 0.025) (Table 4). All other explanatory variables (environmental factors) were not significant (p > 0.05) in this study.

4. Discussion

4.1 Environmental controls on phytoplankton distributions

Tidal fronts, particularly at the boundaries of bank areas, are extremely dynamic at small spatial scales (< 20 km, Landeira et al., 2014). In this study, we sampled across the edge of the Mausund Bank during several tidal phases and, yet, consistent environmental and biological patterns varying along the bank slope were observed. Similar to other bank regions, such as Georges (Franks and Chen, 1996; Hu et al., 2008) and Svalbard Bank (Kędra et al., 2013), primary production in Mausund appears to be stimulated through intensive tidal mixing (particularly in shallow areas). Intrusion of nutrient-rich Atlantic deep waters to the shallow area (here defined as region A) could be an additional explanation for the high

productivity observed in Mausund Bank. The steep bathymetry of the bank edges (Fig. 1b) could promote disruption of internal waves, allowing nutrient-rich deep waters to lift and inject onto the shallow bank through vigorous tidal mixing. The variability of the depth where warmer Atlantic waters were observed at the margin of the bank (St. 3 - 5) (Fig. 3) may indicate lifting of this nutrient-rich water mass, potentially by internal waves or a similar phenomenon. A similar pattern was observed in Georges and Jones Bank (Celtic Sea), where the disruption of internal waves was considered a potential cause for the cross-frontal nutrient transfer from offshore into the bank, explaining the occurrence of long-lasting phytoplankton blooms in the area (Loder et al., 1992; Palmer et al., 2013; Tweddle et al., 2013).

Phytoplankton from distinct regions of Mausund Bank (within and outside the bank) varied in biomass, size structure and in photophysiological status. Large phytoplankton, such as chain-forming diatoms were abundant in un-stratified waters of the bank, whereas the contribution of smaller forms, including flagellates, increased towards the off-bank areas. Again, similar to Georges Bank, chlorophyll *a* and diatom concentrations are high within the bank during spring bloom due to the strong tidal currents flowing over the irregular bathymetry (Franks and Chen, 2001; Townsend and Thomas, 2002). Nutrients are stirred up during pre-bloom conditions, and rapidly assimilated by the phytoplankton once light becomes available (Gallager et al., 1996; Townsend and Thomas, 2002). In the Mausund Bank area, nutrient injection from off-bank Atlantic waters combined with intense tidal mixing might lead to nutrient replenishment, favoring large phytoplankton, such as diatom chains within the bank (as observed in this study). Conversely, density stratification in the region outside the front suppresses nutrients fluxes to the surface, which might have selected for smaller phytoplankton (flagellates) off-bank, as observed in this and other studies (e.g. Georges Bank, Franks and Chen, 2001). Smaller phytoplankton can thrive in low nutrient environments due to a larger surface-to-volume ratio of the cells; and concomitantly, higher

nutrient uptake efficiency resulted from a thinner diffusion boundary layer (Finkel et al., 2009). Even though the contribution of smaller phytoplankton is greater outside the bank, microphytoplankton, particularly diatoms and dinoflagellates, were still dominant, suggesting advection of surface waters and cross-shelf exchange.

Vertical mixing may also explain the predominance of large phytoplankton, such as diatom chains, within Mausund Bank region. Because large chain-forming diatoms would tend to sink faster, given that they are heavier than smaller single cells, turbulence plays an important role in keeping diatoms within the euphotic zone in coastal waters (Landeira et al., 2014; Margalef, 1978). Diatoms in coastal regions are also favored under mixed conditions because increased shear-rate stimulates the diffusion boundary layer, favoring nutrient transport to the cell (Pahlow et al., 1997). Turbulence caused by intense vertical mixing, has been shown to boost cellular enzymatic reactions and enhance nutrient uptake and carbon assimilation in phytoplankton, including diatom chains, when nutrient concentrations start to become limiting (< 3 μM for nitrate+nitrite, similar to the values found in this study), providing an adaptive advantage for growth (Barton et al., 2014).

Strong vertical mixing also explains the presence of spore-forming diatoms, such as *Skeletonema*. During the early spring, friction of tidal currents against the seafloor in the shallow bank region generates turbulence that disturbs bottom sediments. Thus, diatom resting spores are lifted from the sediments and serve as an inoculum to the spring blooms in Norwegian coastal regions (Hegseth et al., 1995). Although, in this study, sampling likely occurred after the onset of the spring bloom (usually in March or April in Norwegian coastal waters, Throndsen et al., 2007), many diatom species, such as *Skeletonema* and *Chaetoceros* found in high abundance in this study are known to form resting spores (Glaucia M. Fragoso et al., 2018; Throndsen et al., 2007; Tomas, 1997). Likewise, benthic diatoms, including *Licmophora* sp., *Pleurosigma* and *Striatella unipunctata* (Throndsen et al., 2007; Tomas,

1997) were observed in the samples, further pointing to the potential role of mixing in stirring up diatoms (and resting spores) from sediments. Similar to Georges Bank, many spore-forming diatoms found in this study, such as *Thalassiosira* sp., *Skeletonema* and *Chaetoceros*, were found blooming in bank regions during spring where intense tidal mixing occurs (Gallager et al., 1996; Gettings et al., 2014).

The saturation values for phytoplankton photosynthesis in Mausund Bank are in agreement with laboratory studies of an isolate of *S. costatum* from the Trondheimsfjord, where cells grown at E_{PAR} of 75 µmol photons m^{-2} s^{-1} at 12 and 24 h day-length, obtained an E_k of 211 µmol photons m^{-2} s^{-1} (Gilstad et al., 1993). However, small changes in E_k were observed, where phytoplankton from well-mixed waters of the inner bank (region A) appeared to require higher light levels to saturate photosynthesis (higher E_k) than the off-bank community. A possible explanation for this pattern is that phytoplankton from this region developed high plasticity to dynamic light environment with fast recovery to the changing light conditions. That is, because the stirring of the water column caused by the tidal fluctuations will result in the phytoplankton cell/chain being moved vertically along an irradiance gradient, and consequently exposed to rapid variation in light levels (Loder and Platt, 1985). Phytoplankton in turbid waters, such as tidal regimes, are known for their ability to adapt to fluctuating light, as opposed to off-shore phytoplankton in clear waters (Brunet et al., 1993; Lavaud et al., 2007). Conversely, the phytoplankton community from off-bank areas appeared to be more sensitive to high light in this study due to their higher ratios of photoprotective xanthophylls, diadinoxanthin and diatoxanthin, per chlorophyll *a* to avoid photodamage (Goss et al., 2006). High diatoxanthin levels observed in phytoplankton from off-bank suggests that the community was experiencing higher light intensities (Moisan et al., 1998).

4.2 SilCam and particle distributions

The application of *in-situ* imaging techniques (e.g. the Video Plankton Recorder) has been used in productive bank areas similar to Mausund Bank, such as Georges Bank (Ashjian et al., 2001; Gallager et al., 1996; Norrbin et al., 1996). Similar to the findings of these studies, plankton distributions were closely related to hydrography, suggesting that the physical environment is the main driver of the vertical distributions of the particles, although micro-scale patchiness (10s of meters) can occur in response to the ability of plankton to search for food (Gallager et al., 1996). Strong vertical mixing within the bank (region A) also explains why particles were able to reach deeper waters in this area. Physical processes at the bottom of the mixed layer (advection, convection, turbulence) can, in some cases, cause particles to escape out of the mixed layer (Noh and Nakada, 2010) and possibly provide food for the benthos in Mausund Bank. Enhanced stratification, as observed in a two-layer system (coastal above Atlantic-related waters) in region B of Mausund Bank could also have trapped particles (diatom chains and fecal pellets, Fig. 8c) at deeper waters (51-100 m). Mass flux of diatoms aggregates to deeper water has been observed in stratified waters subjected to fronts and mesoscale features (Kemp et al., 2006).

In this study, strong horizontal gradients of copepods, fecal pellets, diatom chains and other particles were observed along the bank's edge, being more abundant within the islets and decreasing off-bank. The high abundance of copepods, fecal pellets and ammonium within the bank suggests that copepods were actively grazing in this region. Diatoms as well as aggregates may have stimulated copepod growth, due to the selective feeding behavior of some species towards large particles (option ratio of 1:18) (Hansen et al., 1994; Head and Harris, 1994). However, formation of very large diatom chains, such as those at the upper end

of the prey size spectrum (> 50 µm, see Fig. 2), could also be used as a strategy to avoid predation by zooplankton, although inefficient sloppy feeding behavior in some species can occur (Jansen, 2008). Modulation of chain size (either from small to large size of the prey spectrum) has been reported as an important ecological trait driving phytoplankton species competition because it influences size plasticity, allowing the prey to escape the optimum grazing size spectrum (Bergkvist et al., 2012; Bjærke et al., 2015; Landeira et al., 2014).

Most particles (~87% of total counts) observed by the SilCam classified as 'other' in this study. This category contained particles, such as bio-aggregates and marine snow. Intensive mixing within the bank area might have promoted the aggregation of particles, particularly of phytodetritus (either dead phytoplankton or tightly packed in fecal pellets) because turbulent shear can cause their intensive collision (Burd and Jackson, 2009). Moreover, phytoplankton, particularly diatoms, can enhance flocculation via production of Extracellular Polymeric Substances (EPS), which have sticky surface properties that ensure high likelihood of coalescence between particles following a collision (Alldredge et al., 1993; Thorton, 2002). Diatoms are known to form aggregates towards the end of the bloom formation; and many species, including those found in this study (*Chaetoceros*, *Skeletonema* and *Thalassiosira*) are known to contribute largely to EPS formation (Thorton, 2002). Phytoplankton and particle dynamics across Mausund Bank are summarized in Figure 10.

The deployment of the suite of particle monitoring tools on the profiling frame from the vessel is an excellent method to obtain high temporal resolution profiles from a single station. However, integration of particle monitoring sensors on-board autonomous vehicles could improve spatio-temporal sampling to wider scales due to the high variability of plankton communities (Ludvigsen et al., 2018). In addition, imaging smaller particles using similar techniques to that of the SilCam could provide valuable information on the phytoplankton composition. Incorporation of *in-situ* flow cytometry (Sosik and Olson, 2007),

coupled to a lower magnification SilCam, and mounted on an autonomous platform could provide a possible solution.

5. Conclusion

Phytoplankton from distinct regions of Mausund Bank (within and outside the islets) varied in concentration, size and photophysiological status. Large phytoplankton (> 20 µm), such as chain-forming diatoms were abundant in un-stratified waters of the bank, whereas the contribution of small phytoplankton (< 20 µm), such as flagellates increased towards off-bank. Vertical mixing may also explain the predominance of larger (chain-forming) phytoplankton, such as spore-forming blooming diatoms. In spite of deeper mixing, phytoplankton from waters of the inner bank (region A) required more light to saturate photosynthesis (higher E_k) than the off-bank community, possibly because of high plasticity to dynamic light environment. Conversely, the phytoplankton community from the off-bank were more exposed to higher irradiance than at the inner bank indicated by higher cellular concentrations of photoprotective pigments, particularly diatoxanthin used in the xanthophyll cycle to cope with photo-damage. The large abundance of copepods, fecal pellets and ammonium within the bank suggests that copepods were actively grazing on the microphytoplankton. Intensive mixing is suggested to have promoted the agglomeration of particles, such as marine snow, within the bank.

6. Acknowledgements

We would like to thank the crew of the *R/V Gunnerus* and the support of technicians and scientists involved in the cruise. Many thanks to Odd Arne Arnesen from the Mausund field Station (http://www.eider.no/) for his logistical help with sampling and accommodation

during field work. All authors were funded by the Norwegian Research Council (NRC, Project ENTiCE, 255303). Contributions by G.J. are from the Center of Excellence for Autonomous Marine Operations and Systems (AMOS) at NTNU (NRC, Project 223254).

7. Authors contributions

G.M.F. designed the study, analyzed the pigment data, performed the statistics and wrote the initial draft of the manuscript. E.J.D. collected and analyzed the *in-situ* imaging data. G.M.F, I.E., G.J. and K.B.S. collected the discrete water samples at sea. G.J. performed the photosynthesis versus irradiance experiments. M.S.C. and K.B.S. identified the phytoplankton species in the microscope and provided a species list. T.F., M.L. and K.R. designed AUV sampling strategy and analyzed the AUV data. I.E. and G.J. supervised the study. All authors contributed substantially to posterior drafting of the manuscript, provided critical comments and approved the final submitted version.

8. Conflict of interest

The authors have no conflict or declaration of interest.

9. References

Abadi, M., Barham, P., Chen, J., Chen, Z., Davis, A., Dean, J., Devin, M., Ghemawat, S., Irving, G., Isard, M., Kudlur, M., Levenberg, J., Monga, R., Moore, S., Murray, D.G., Steiner, B., Tucker, P., Vasudevan, V., Warden, P., Wicke, M., Yu, Y., Zheng, X., Brain, G., 2016. TensorFlow: A System for Large-Scale Machine Learning TensorFlow: A system for large-scale machine learning, in: 12th USENIX Symposium on Operating Systems Design and Implementation (OSDI '16). https://doi.org/10.1038/nn.3331

Acevedo-Trejos, E., Brandt, G., Merico, A., Smith, S.L., 2013. Biogeographical patterns of phytoplankton community size structure in the oceans. Glob. Ecol. Biogeogr. 22, 1060–1070. https://doi.org/10.1111/geb.12071

Alldredge, A.L., Passow, U., Logan, B.E., 1993. The abundance and significance of a class of large, transparent organic particles in the ocean. Deep Sea Res. Part I Oceanogr. Res. Pap. 40, 1131–1140. https://doi.org/10.1016/0967-0637(93)90129-Q

Ashjian, C.J., Davis, C.S., Gallager, S.M., Alatalo, P., 2001. Distribution of plankton, particles, and hydrographic features across Georges Bank described using the Video Plankton Recorder. Deep. Res. Part II Top. Stud. Oceanogr. 48, 245–282. https://doi.org/10.1016/S0967-0645(00)00121-1

Barrett, J., Jeffrey, S.W., 1971. A note on the occurrence of chlorophyllase in marine algae. J. Exp. Mar. Bio. Ecol. 7, 255–262. https://doi.org/10.1016/0022-0981(71)90008-6

Barrett, R.., Rov, N., Loen, J., Montevecchi, W.A., 1990. Diets of shags Phalacrocorax aristotelis and cormorants P carbo in Norway and possible implications for gadoid stock recruitment. Mar. Ecol. Prog. Ser. 66, 205–218. https://doi.org/10.3354/meps066205

Barton, A.D., Ward, B.A., Williams, R.G., Follows, M.J., 2014. The impact of fine-scale turbulence on phytoplankton community structure. Limnol. Oceanogr. Fluids Environ. 4, 34–49. https://doi.org/10.1215/21573689-2651533

Bergkvist, J., Thor, P., Jakobsen, H.H., Wängberg, S.-Å., Selander, E., 2012. Grazer-induced chain length plasticity reduces grazing risk in a marine diatom. Limnol. Oceanogr. 57, 318–324. https://doi.org/10.4319/lo.2012.57.1.0318

Bjærke, O., Jonsson, P.R., Alam, A., Selander, E., 2015. Is chain length in phytoplankton regulated to evade predation? J. Plankton Res. 37, fbv076. https://doi.org/10.1093/plankt/fbv076

Boss, E., Guidi, L., Richardson, M.J., Stemmann, L., Gardner, W., Bishop, J.K.B., Anderson, R.F., Sherrell, R.M., 2015. Optical techniques for remote and in-situ characterization of particles pertinent to GEOTRACES. Prog. Oceanogr. 133, 43–54. https://doi.org/10.1016/j.pocean.2014.09.007

Bouman, H.A., Platt, T., Doblin, M., Figueiras, F.G., Gudmundsson, K., Gudfinnsson, H.G., Huang, B., Hickman, A., Hiscock, M., Jackson, T., Lutz, V.A., Mélin, F., Rey, F., Pepin, P., Segura, V., Tilstone, G.H., van Dongen-Vogels, V., Sathyendranath, S., 2018. Photosynthesis–irradiance parameters of marine phytoplankton: synthesis of a global data set. Earth Syst. Sci. Data 10, 251–266. https://doi.org/10.5194/essd-10-251-2018

Boyd, P.W., Strzepek, R., Takeda, S., Jackson, G., Wong, C.S., McKay, R.M., Law, C., Kiyosawa, H., Saito, H., Sherry, N., Johnson, K., Gower, J., Ramaiah, N., 2005. The

evolution and termination of an iron-induced mesoscale bloom in the northeast subarctic Pacific. Limnol. Oceanogr. 50, 1872–1886. https://doi.org/10.4319/lo.2005.50.6.1872

Brunet, C., Brylinski, J.M., Lemoine, Y., 1993. In situ variations of the xanthophylls diatoxanthin and diadinoxanthin - Photoadaptation and relationships with a hydrodynamical system in the eastern English Channel. Mar. Ecol. Prog. Ser. 102, 69–78. https://doi.org/10.3354/meps102069

Burd, A.B., Jackson, G.A., 2009. Particle Aggregation. Ann. Rev. Mar. Sci. 1, 65–90. https://doi.org/10.1146/annurev.marine.010908.163904

Cavan, E.L., Le Moigne, F.A.C., Poulton, A.J., Tarling, G.A., Ward, P., Daniels, C.J., Fragoso, G.M., Sanders, R.J., 2015. Attenuation of particulate organic carbon flux in the Scotia Sea, Southern Ocean, is controlled by zooplankton fecal pellets. Geophys. Res. Lett. 42, 821–830. https://doi.org/10.1002/2014GL062744.Received

Clarke, K.R., Warwick, R.M., 2001. Change in marine communities: an approach to statistical analysis and interpretation, 2nd Editio. ed. PRIMER-E, Plymouth.

Cross, J., Nimmo-Smith, W.A.M., Hosegood, P.J., Torres, R., 2014. The dispersal of phytoplankton populations by enhanced turbulent mixing in a shallow coastal sea. J. Mar. Syst. 136, 55–64. https://doi.org/10.1016/j.jmarsys.2014.03.009

Davies, E.J., Ahnell, A., Leirvik, F., Brandvik, P.J., 2018. Optical Monitoring of Subsea Blowout Droplets and Subsea Dispersant Efficacy, in: Proceedings of the Forty-First AMOP Technical Seminar, Proceedings of the Forty-First AMOP Technical Seminar, Environment and Climate Change Canada. Ottawa, ON, pp. 90–111.

Davies, E.J., Brandvik, P.J., Leirvik, F., Nepstad, R., 2017. The use of wide-band transmittance imaging to size and classify suspended particulate matter in seawater. Mar. Pollut. Bull. 115, 105–114. https://doi.org/10.1016/j.marpolbul.2016.11.063

Davies, E.J., Nepstad, R., 2017. In situ characterisation of complex suspended particulates surrounding an active submarine tailings placement site in a Norwegian fjord. Reg. Stud. Mar. Sci. 16, 198–207. https://doi.org/10.1016/j.rsma.2017.09.008

Ding, H., Wei, B., Tang, N., Yu, Z., Wang, N., Zheng, H., Zheng, B., 2018. Plankton Image Classification via Multi-Class Imbalanced Learning, in: 2018 OCEANS - MTS/IEEE Kobe Techno-Oceans (OTO). IEEE, pp. 1–6. https://doi.org/10.1109/OCEANSKOBE.2018.8559238

Egeland, E., Garrido, J., Clementson, L., Andresen, K., Thomas, C., Zapata, M., Airs, R., LLewellyn, C.A., Newman, G.L., Rodríguez, F., Roy, S., 2011. Data sheets aiding identification of phytoplankton carotenoids and chlorophylls., in: Roy, S., Llewellyn, C.A., Egeland, E., Johnsen, G. (Eds.), Phytoplankton Pigments: Characterization, Chemotaxonomy and Applications in Oceanography. Cambridge Environmental Chemistry Series, Cambridge: Cambridge University Press., pp. 665–674.

Ervik, H., Finne, T.E., Jenssen, B.M., 2018. Toxic and essential elements in seafood from Mausund, Norway. Environ. Sci. Pollut. Res. 25, 7409–7417. https://doi.org/10.1007/s11356-017-1000-4

Finkel, Z. V., Beardall, J., Flynn, K.J., Quigg, A., Rees, T.A. V., Raven, J.A., 2009. Phytoplankton in a changing world: cell size and elemental stoichiometry. J. Plankton Res. 32, 119–137. https://doi.org/10.1093/plankt/fbp098

Fossum, T.O., Eidsvik, J., Ellingsen, I., Alver, M.O., Fragoso, G.M., Johnsen, G., Mendes, R., Ludvigsen, M., Rajan, K., 2018. Information-driven robotic sampling in the coastal ocean. J. F. Robot. 1–21. https://doi.org/10.1002/rob.21805

Fossum, T.O., Fragoso, G.M., Davies, E.J., Ullgren, J.E., Mendes, R., Johnsen, G., Ellingsen, I., Eidsvik, J., Ludvigsen, M., Rajan, K., 2019. Toward adaptive robotic sampling of phytoplankton in the coastal ocean. Sci. Robot. 4, eaav3041. https://doi.org/10.1126/scirobotics.aav3041

Fragoso, G.M., Poulton, A.J., Pratt, N., Johnsen, G., Purdie, D.A., 2018. Trait-based analysis of subpolar North Atlantic phytoplankton and plastidic ciliate communities using automated flow cytometer. Limnol. Oceanogr. in review.

Fragoso, G.M., Poulton, A.J., Yashayaev, I.M., Head, E.J.H., Johnsen, G., Purdie, D.A., 2018. Diatom Biogeography From the Labrador Sea Revealed Through a Trait-Based Approach. Front. Mar. Sci. 5. https://doi.org/10.3389/fmars.2018.00297

Fragoso, G.M., Poulton, A.J., Yashayaev, I.M., Head, E.J.H., Stinchcombe, M.C., Purdie, D.A., 2016. Biogeographical patterns and environmental controls of phytoplankton communities from contrasting hydrographical zones of the Labrador Sea. Prog. Oceanogr. 141, 212–226. https://doi.org/10.1016/j.pocean.2015.12.007

Franks, P.J.S., Chen, C., 2001. A 3-D prognostic numerical model study of the Georges bank ecosystem. Part II: biological–physical model. Deep Sea Res. Part II Top. Stud. Oceanogr. 48, 457–482. https://doi.org/10.1016/S0967-0645(00)00125-9

Franks, P.J.S., Chen, C., 1996. Plankton production in tidal fronts: A model of Georges Bank in summer. J. Mar. Res. 54, 631–651. https://doi.org/10.1357/0022240963213718

Gallager, S.M., Davis, C.S., Epstein, A.W., Solow, A., Beardsley, R.C., 1996. High-resolution observations of plankton spatial distributions correlated with hydrography in the Great South Channel, Georges Bank. Deep. Res. Part II Top. Stud. Oceanogr. 43, 1627–1663. https://doi.org/10.1016/S0967-0645(96)00058-6

Gettings, R.M., Townsend, D.W., Thomas, M.A., Karp-Boss, L., 2014. Dynamics of late spring and summer phytoplankton communities on Georges Bank, with emphasis on diatoms, Alexandrium spp., and other dinoflagellates. Deep Sea Res. Part II Top. Stud. Oceanogr. 103, 120–138. https://doi.org/10.1016/j.dsr2.2013.05.012

Gilstad, M., Johnsen, G., Sakshaug, E., 1993. Photosynthetic parameters, pigment composition and respiration rates of the marine diatom Skeletonema costatum grown in continuous light and a 12:12 h light-dark cycle. J. Plankton Res. 15, 939–951. https://doi.org/10.1093/plankt/15.8.939

Goss, R., Ann Pinto, E., Wilhelm, C., Richter, M., 2006. The importance of a highly active and ΔpH-regulated diatoxanthin epoxidase for the regulation of the PS II antenna function in diadinoxanthin cycle containing algae. J. Plant Physiol. 163, 1008–1021. https://doi.org/10.1016/j.jplph.2005.09.008

Guidi, L., Stemmann, L., Jackson, G.A., Ibanez, F., Claustre, H., Legendre, L., Picheral, M., Gorsky, G., 2009. Effects of phytoplankton community on production, size and export of large aggregates: A world-ocean analysis. Limnol. Oceanogr. 54, 1951–1963. https://doi.org/10.4319/lo.2009.54.6.1951

Hansen, B., Bjornsen, P.K., Hansen, P.J., 1994. The size ratio between planktonic predators

and their prey Prey size (pm ESD). Limnol. Oceanogr. 39, 395–403.

Head, E., Harris, L., 1994. Feeding selectivity by copepods grazing on natura: mixtures of phytoplankton determined by HPLC analysis of pigments. Mar. Ecol. Prog. Ser. 110, 75–83. https://doi.org/10.3354/meps110075

Hegseth, E.N., Svendsen, H., von Quillfeldt, C.H., 1995. Phytoplankton in fjords and coastal waters of northern Norway: environmental conditions and dynamics of the spring bloom. Ecol. Fjords Coast. Waters 45–72.

Higgins, H.W., Wright, S.W., Schlüter, L., 2011. Quantitative interpretation of chemotaxonomic pigment data, in: Roy, S., Llewellyn, C., Egeland, E.S., Johnsen, G. (Eds.), Phytoplankton Pigments: Characterization, Chemotaxonomy and Applications in Oceanography. Cambridge University Press, Cambridge, pp. 257–313. https://doi.org/10.1017/CBO9780511732263.010

Holm-Hansen, O., Riemann, B., 1978. Chlorophyll a Determination: Improvements in Methodology. Oikos 30, 438. https://doi.org/10.2307/3543338

Hu, Q., Davis, C., 2006. Accurate automatic quantification of taxa-specific plankton abundance using dual classification with correction. Mar. Ecol. Prog. Ser. 306, 51–61. https://doi.org/10.3354/meps306051

Hu, S., Townsend, D.W., Chen, C., Cowles, G., Beardsley, R.C., Ji, R., Houghton, R.W., 2008. Tidal pumping and nutrient fluxes on Georges Bank: A process-oriented modeling study. J. Mar. Syst. 74, 528–544. https://doi.org/10.1016/j.jmarsys.2008.04.007

Jansen, S., 2008. Copepods grazing on Coscinodiscus wailesii: a question of size? Helgol. Mar. Res. 62, 251–255. https://doi.org/10.1007/s10152-008-0113-z

Jassby, A.D., Platt, T., 1976. Mathematical formulation of the relationship between photosynthesis and light for phytoplankton. Limnol. Oceanogr. 21, 540–547. https://doi.org/10.4319/lo.1976.21.4.0540

Jeffrey, S., Hallegraeff, G., 1987. Chlorophyllase distribution in ten classes of phytoplankton: a problem for chlorophyll analysis. Mar. Ecol. Prog. Ser. 35, 293–304. https://doi.org/10.3354/meps035293

Jeffrey, S.W., Mantoura, R.F.C., Wright, S.W., 1997. Phytoplankton Pigments in Oceanography. SCOR and UNESCO, Paris.

Jeffrey, S.W., Vesk, M., 1997. Introduction to marine phytoplankton and their pigment signatures., in: Jeffrey, S.W., Mantoura, R.F.C., Wright, S.W. (Eds.), Phytoplankton Pigments in Oceanography: Guidelines to Modern Methods. UNESCO, Paris, pp. 19–36.

Jenssen, B.M., Åsmul, J.I., Ekker, M., Vongraven, D., 2010. To go for a swim or not? Consequences of neonatal aquatic dispersal behaviour for growth in grey seal pups. Anim. Behav. 80, 667–673. https://doi.org/10.1016/j.anbehav.2010.06.028

Johnsen, G., Moline, M.A., Pettersson, L.H., Pinckney, J., Pozdnyakov, D. V., Egeland, E.S., Schofield, O.M., 2011. Optical monitoring of phytoplankton bloom pigment signatures, in: Roy, S., Llewellyn, C., Egeland, E.S., Johnsen, G. (Eds.), Phytoplankton Pigments. Cambridge University Press, Cambridge, pp. 538–606. https://doi.org/10.1017/CBO9780511732263.020

Johnsen, G., Norli, M., Moline, M., Robbins, I., von Quillfeldt, C., Sørensen, K., Cottier, F., Berge, J., 2018. The advective origin of an under-ice spring bloom in the Arctic Ocean using multiple observational platforms. Polar Biol. https://doi.org/10.1007/s00300-018-2278-5

Johnsen, G., Sakshaug, E., 2007. Biooptical characteristics of PSII and PSI in 33 species (13 pigment groups) of marine phytoplankton, and the relevance for pulse-amplitude-modulated and fast-repetition-rate fluorometry 1. J. Phycol. 43, 1236–1251. https://doi.org/10.1111/j.1529-8817.2007.00422.x

Johnsen, G., Sakshaug, E., 1993. BIO-OPTICAL CHARACTERISTICS AND PHOTOADAPTIVE RESPONSES IN THE TOXIC AND BLOOM-FORMING DINOFLAGELLATES GYRODINIUM AUREOLUM, GYMNODINIUM GALATHEANUM , AND TWO STRAINS OF PROROCENTRUM MINIMUM 1. J. Phycol. 29, 627–642. https://doi.org/10.1111/j.0022-3646.1993.00627.x

Julshamn, K., Duinker, A., Frantzen, S., Torkildsen, L., Maage, A., 2008. Organ Distribution and Food Safety Aspects of Cadmium and Lead in Great Scallops, Pecten maximus L., and Horse Mussels, Modiolus modiolus L., from Norwegian Waters. Bull. Environ. Contam. Toxicol. 80, 385–389. https://doi.org/10.1007/s00128-008-9377-x

Kędra, M., Renaud, P.E., Andrade, H., Goszczko, I., Ambrose, W.G., 2013. Benthic community structure, diversity, and productivity in the shallow Barents Sea bank (Svalbard Bank). Mar. Biol. 160, 805–819. https://doi.org/10.1007/s00227-012-2135-y

Kemp, A.E.S., Pearce, R.B., Grigorov, I., Rance, J., Lange, C.B., Quilty, P., Salter, I., 2006. Production of giant marine diatoms and their export at oceanic frontal zones: Implications for Si and C flux from stratified oceans. Global Biogeochem. Cycles 20, n/a-n/a. https://doi.org/10.1029/2006GB002698

Kiørboe, T., 1993. Turbulence, Phytoplankton Cell Size, and the Structure of Pelagic Food Webs. pp. 1–72. https://doi.org/10.1016/S0065-2881(08)60129-7

Landeira, J.M., Ferron, B., Lunven, M., Morin, P., Marié, L., Sourisseau, M., 2014. Biophysical Interactions Control the Size and Abundance of Large Phytoplankton Chains at the Ushant Tidal Front. PLoS One 9, e90507. https://doi.org/10.1371/journal.pone.0090507

Laurenceau-Cornec, E., Trull, T., Davies, D., De La Rocha, C., Blain, S., 2015. Phytoplankton morphology controls on marine snow sinking velocity. Mar. Ecol. Prog. Ser. 520, 35–56. https://doi.org/10.3354/meps11116

Lavaud, J., Rousseau, B., Etienne, A.L., 2004. General features of photoprotection by energy dissipation in planktonic diatoms (Bacillariophyceae). J. Phycol. 40, 130–137. https://doi.org/10.1046/j.1529-8817.2004.03026.x

Lavaud, J., Strzepek, R.F., Kroth, P.G., 2007. Photoprotection capacity differs among diatoms: Possible consequences on the spatial distribution related to fluctuations in the underwater light climate. Limnol. Oceanogr. 52, 1188–1194. https://doi.org/10.4319/lo.2007.52.3.1188

Lehmuskero, A., Skogen Chauton, M., Boström, T., 2018. Light and photosynthetic microalgae: A review of cellular- and molecular-scale optical processes. Prog. Oceanogr. 168, 43–56. https://doi.org/10.1016/j.pocean.2018.09.002

Li, W.K.W., 2002. Macroecological patterns of phytoplankton in the northwestern North Atlantic Ocean. Nature 419, 154–157. https://doi.org/10.1038/nature00983.1.

Loder, J.W., Brickman, D., Horne, E.P.W., 1992. Detailed structure of currents and hydrography on the northern side of Georges Bank. J. Geophys. Res. 97, 14331. https://doi.org/10.1029/92JC01342

Loder, J.W., Platt, T., 1985. Physical controls on phytoplankton production at tidal fronts, in: Gibbs, P.E. (Ed.), Proceedings of the 19th European Marine Biological Symposium. Cambridge University Press, pp. 3–21.

Lorentsen, S.-H., Sjøtun, K., Grémillet, D., 2010. Multi-trophic consequences of kelp harvest. Biol. Conserv. 143, 2054–2062. https://doi.org/10.1016/j.biocon.2010.05.013

Ludvigsen, M., Berge, J., Geoffroy, M., Cohen, J.H., De La Torre, P.R., Nornes, S.M., Singh, H., Sørensen, A.J., Daase, M., Johnsen, G., 2018. Use of an Autonomous Surface Vehicle reveals small-scale diel vertical migrations of zooplankton and susceptibility to light pollution under low solar irradiance. Sci. Adv. 4, eaap9887. https://doi.org/10.1126/sciadv.aap9887

Marañón, E., 2009. Phytoplankton Size Structure, in: Encyclopedia of Ocean Sciences. Elsevier, pp. 445–452. https://doi.org/10.1016/B978-012374473-9.00661-5

Margalef, R., 1978. Life-forms of phytoplankton as survival alternatives in an unstable environment. Oceanol. Acta 1, 493–509. https://doi.org/10.1007/BF00202661

Maury, O., Shin, Y.-J., Faugeras, B., Ben Ari, T., Marsac, F., 2007. Modeling environmental effects on the size-structured energy flow through marine ecosystems. Part 2: Simulations. Prog. Oceanogr. 74, 500–514. https://doi.org/10.1016/j.pocean.2007.05.001

Moisan, T.A., Olaizola, M., Mitchell, B.G., 1998. Xanthophyll cycling in *Phaeocystis antarctica*: Changes in cellular fluorescence. Mar. Ecol. Prog. Ser. 169, 113–121. https://doi.org/10.3354/meps169113

Möller, K., St John, M., Temming, A., Floeter, J., Sell, A., Herrmann, J., Möllmann, C., 2012. Marine snow, zooplankton and thin layers: indications of a trophic link from small-scale sampling with the Video Plankton Recorder. Mar. Ecol. Prog. Ser. 468, 57–69. https://doi.org/10.3354/meps09984

Mouw, C.B., Barnett, A., Mckinley, G.A., Gloege, L., Pilcher, D., 2016. Global Biogeochemical Cycles in the global ocean 1–21. https://doi.org/10.1002/2015GB005355.Received

Noh, Y., Nakada, S., 2010. Estimation of the particle flux from the convective mixed layer by large eddy simulation. J. Geophys. Res. Ocean. 115, 1–7. https://doi.org/10.1029/2009JC005669

Norrbin, M.F., Vis, C.S.D.A., Gallager, S.M., 1996. Differences in fine-scale structure and composition of zooplankton between mixed and stratified regions of Georges Bank. Deep. Res. Part II Top. Stud. Oceanogr. 43, 1905–1924. https://doi.org/10.1016/S0967-0645(96)00046-X

Nymark, M., Valle, K.C., Brembu, T., Hancke, K., Winge, P., Andresen, K., Johnsen, G., Bones, A.M., 2009. An Integrated Analysis of Molecular Acclimation to High Light in the Marine Diatom Phaeodactylum tricornutum. PLoS One 4, e7743.

https://doi.org/10.1371/journal.pone.0007743

Pahlow, M., Riebesell, U., Wolf-Gladrow, D. a., 1997. Impact of cell shape and chain formation on nutrient acquisition by marine diatoms. Limnol. Oceanogr. 42, 1660–1672. https://doi.org/10.4319/lo.1997.42.8.1660

Palmer, M.R., Inall, M.E., Sharples, J., 2013. The physical oceanography of Jones Bank: A mixing hotspot in the Celtic Sea. Prog. Oceanogr. 117, 9–24. https://doi.org/10.1016/j.pocean.2013.06.009

Poulton, A.J., Holligan, P.M., Hickman, A., Kim, Y.N., Adey, T.R., Stinchcombe, M.C., Holeton, C., Root, S., Woodward, E.M.S., 2006. Phytoplankton carbon fixation, chlorophyll-biomass and diagnostic pigments in the Atlantic Ocean. Deep. Res. Part II Top. Stud. Oceanogr. 53, 1593–1610. https://doi.org/10.1016/j.dsr2.2006.05.007

Reynolds, R.A., Stramski, D., Wright, V.M., Woźniak, S.B., 2010. Measurements and characterization of particle size distributions in coastal waters. J. Geophys. Res. 115, C08024. https://doi.org/10.1029/2009JC005930

Rodríguez, F., Chauton, M., Johnsen, G., Andresen, K., Olsen, L.M., Zapata, M., 2006. Photoacclimation in phytoplankton: implications for biomass estimates, pigment functionality and chemotaxonomy. Mar. Biol. 148, 963–971. https://doi.org/10.1007/s00227-005-0138-7

Roy, S., Chanut, J.P., Gosselin, M., Sime-Ngando, T., 1996. Characterization of phytoplankton communities in the lower St. LawrenceEstuary using HPLC-detected pigments and cell microscopy. Mar. Ecol. Prog. Ser. 142, 55–73. https://doi.org/10.3354/meps142055

Rykaczewski, R.R., Checkley, D.M., 2008. Influence of ocean winds on the pelagic ecosystem in upwelling regions. Proc. Natl. Acad. Sci. 105, 1965–1970. https://doi.org/10.1073/pnas.0711777105

Sætre, R., 2007. Driving forces in the Norwegian Coastal Current. The Norwegian Coastal Current— Oceanography and Climate., in: Sætre, R. (Ed.), The Norwegian Coastal Current— Oceanography and Climate. Tapir Academic Press, Trondheim., p. 89–98.

Salter, I., Lampitt, R.S., Sanders, R., Poulton, A., Kemp, A.E.S., Boorman, B., Saw, K., Pearce, R., 2007. Estimating carbon, silica and diatom export from a naturally fertilised phytoplankton bloom in the Southern Ocean using PELAGRA: A novel drifting sediment trap. Deep Sea Res. Part II Top. Stud. Oceanogr. 54, 2233–2259. https://doi.org/10.1016/j.dsr2.2007.06.008

Skagseth, Ø., Drinkwater, K.F., Terrile, E., 2011. Wind- and buoyancy-induced transport of the Norwegian Coastal Current in the Barents Sea. J. Geophys. Res. 116, C08007. https://doi.org/10.1029/2011JC006996

Sosik, H.M., Olson, R.J., 2007. Automated taxonomic classification of phytoplankton sampled with imaging-in-flow cytometry. Limnol. Oceanogr. Methods 5, 204–216. https://doi.org/10.4319/lom.2007.5.204

Sousa, A., Madureira, L., Coelho, J., Pinto, J., Pereira, J., Borges Sousa, J., Dias, P., 2012. LAUV: The Man-Portable Autonomous Underwater Vehicle. IFAC Proc. Vol. 45, 268–274. https://doi.org/10.3182/20120410-3-PT-4028.00045

Stemmann, L., Boss, E., 2012. Plankton and Particle Size and Packaging: From Determining

Optical Properties to Driving the Biological Pump. Ann. Rev. Mar. Sci. 4, 263–290. https://doi.org/10.1146/annurev-marine-120710-100853

Suzuki, R., Fujita, Y., 1986. Chlorophyll decomposition in Skeletonema costatum: a problem in chlorophyll determination of water samples. Mar. Ecol. Prog. Ser. 28, 81–85. https://doi.org/10.3354/meps028081

Thorton, D.C.O., 2002. Diatom aggregation in the sea: mechanisms and ecological implications. Eur. J. Phycol. 37, S0967026202003657. https://doi.org/10.1017/S0967026202003657

Throndsen, J., Hasle, G.R., Tangen, K., 2007. Phytoplankton of Norwegian coastal waters. Almater Forlag AS.

Tiller, R.G., Hansen, L., Richards, R., Strand, H., 2015. Work segmentation in the Norwegian salmon industry: The application of segmented labor market theory to work migrants on the island community of Frøya, Norway. Mar. Policy 51, 563–572. https://doi.org/10.1016/j.marpol.2014.10.001

Tomas, C.R., 1997. Identifying marine phytoplankton. Academic press.

Townsend, D., Thomas, M., 2002. Springtime nutrient and phytoplankton dynamics on Georges Bank. Mar. Ecol. Prog. Ser. 228, 57–74. https://doi.org/10.3354/meps228057

Tréguer, P., Bowler, C., Moriceau, B., Dutkiewicz, S., Gehlen, M., Aumont, O., Bittner, L., Dugdale, R., Finkel, Z., Iudicone, D., Jahn, O., Guidi, L., Lasbleiz, M., Leblanc, K., Levy, M., Pondaven, P., 2018. Influence of diatom diversity on the ocean biological carbon pump. Nat. Geosci. 11, 27–37. https://doi.org/10.1038/s41561-017-0028-x

Tweddle, J.F., Sharples, J., Palmer, M.R., Davidson, K., McNeill, S., 2013. Enhanced nutrient fluxes at the shelf sea seasonal thermocline caused by stratified flow over a bank. Prog. Oceanogr. 117, 37–47. https://doi.org/10.1016/j.pocean.2013.06.018

Uitz, J., Claustre, H., Morel, A., Hooker, S.B., 2006. Vertical distribution of phytoplankton communities in open ocean: An assessment based on surface chlorophyll. J. Geophys. Res. 111, C08005. https://doi.org/10.1029/2005JC003207

Uitz, J.U., Huot, Y., Bruyant, F., Babin, M., Claustre, H., 2008. Relating phytoplankton photophysiological properties to community structure on large scales. Limnol. Oceanogr. 53, 614–630. https://doi.org/10.4319/lo.2008.53.2.0614

Vidussi, F., Claustre, H., Manca, B.B., Luchetta, A., Jean-Claude, M., 2001. Phytoplankton pigment distribution in relation to upper Francesca Claustre For the whole Tchl a concentration mg estimated production value being mg m and the highest picophytoplankton contribution of Tchl a •. gyres by low Tchl a concentrations and. J. Geophys. Res. 106, 939–956. https://doi.org/10.1029/1999JC000308

Vidussi, F., Roy, S., Lovejoy, C., Gammelgaard, M., Thomsen, H.A., Booth, B., Tremblay, J.-E., Mostajir, B., 2004. Spatial and temporal variability of the phytoplankton community structure in the North Water Polynya, investigated using pigment biomarkers. Can. J. Fish. Aquat. Sci. 61, 2038–2052. https://doi.org/10.1139/f04-152

Volent, Z., 2011. Improved monitoring of phytoplankton bloom dynamics in a Norwegian fjord by integrating satellite data, pigment analysis, and Ferrybox data with a coastal observation network. J. Appl. Remote Sens. 5, 053561. https://doi.org/10.1117/1.3658032

Zapata, M., Rodríguez, F., Garrido, J., 2000. Separation of chlorophylls and carotenoids from marine phytoplankton:a new HPLC method using a reversed phase C8 column and pyridine-containing mobile phases. Mar. Ecol. Prog. Ser. 195, 29–45. https://doi.org/10.3354/meps195029

Figure 1. Map showing the a) Froan archipelago in the coast of Norway and the b) stations sampled (1-5), where discrete water sampling and vertical *in-situ* profiling occurred on-board of the *R/V Gunnerus*, in addition to L-AUV sampling transects performed at region A (TA, within the bank) and region B (TB, off-bank).

Figure 2. Collages of particle images from 1-5m (left) and 5-70 m (right) from a,b) station 2 and c,d) station 5 obtained from the Silhouette Camera (SilCam). The collages of particle images are auto-generated using a packaging algorithm that attempts to represent the size distribution of particles to correspond with what was measured, but in doing do, concentration (or separation between particles) is not represented.

Figure 3. Vertical profiles of a) temperature (ºC), b) salinity, c) density (σ_Θ, kg m^{-3}) and d) stratification index (SI, kg m^{-4}) of stations 1-5.

Figure 4. a) L-AUV transects (gray lines) and key environmental variables in region A (TA) and B (TB). Vertical profiles of environmental variables, including b-c) temperature and d-e) salinity, in addition to biological variables, such as concentrations of f-g) chlorophyll *a* (mg Chl$a_{\text{in-situ}}$ m^{-3}) h-i) colored dissolved organic matter (CDOM, ppm) and j-k) and total suspended matter (TSM, measured as b_b at 700 nm, m^{-1}) along transects A (left) and B (right) from a fixed reference position shown by the star in Figure 3a (x-axis).

Figure 5. a) Non-metric multi-dimensional scaling (nMDS) plot representing the similarity of phytoplankton size structure as a function of a) samples from different depths (< 5 m, circles,

25 m, triangle, 40 m, square) and stations (1-5, also denoted with different colors) and b) relative proportion of size classes: nano- + picopytoplakton (N_f+P_f) and microphytoplankton (M_f, white).

Figure 6. Pooled photosynthesis-irradiance curves of phytoplankton from stations 1-5, showing the electron transport rate (µmol electrons m^{-2} s^{-1}, y-axis) as a function of irradiance (E_{PAR} in µmol photons m^{-2} s^{-1}, x-axis). Line indicate the fit of the curves from grouping of the following stations: 1 and 2 (solid), 3 (dotted) and 4 and 5 (dashed). Average values of photosynthethic parameters per station for each curve are shown in Table 3.

Figure 7. Vertical distribution of particle counts per volume of seawater sampled (× 10^3 counts m^{-3}) derived from the Silhouette Camera (SilCam) at stations 1-5: a) copepods, b) fecal pellets, diatom chains and other particles from stations 1-5.

Figure 8. Average particle volume concentration per volume of seawater sampled (cm^3 m^{-3}) derived from the Silhouette Camera (SilCam) for copepods (black), fecal pellets (gray) and diatom chains (white) from a) surface/subsurface (1-20 m), b) mid-depth (21-50 m) and deep waters (51-100 m) from stations 1-5.

Figure 9. Ordination diagram generated from redundancy analysis (RDA). Triplot represents phytoplankton size fraction (black lines), explanatory environmental variables (red lines), supplementary variables (blue lines) and samples for each depth and station (closed circles; colors refers to stations at Figure 1). Phytoplankton size fractions: MICRO =

microphytoplankton, NANO + PICO = nano- + picophytoplankton. Environmental variables: NH4 = ammonium, NO3+NO2 = nitrate and nitrite, Si(OH)4 = silicate, PO4 = phosphate, SI = stratification index. Supplementary variables: ChlaFluor = fluorometric-derived chlorophyll *a*, FECAL = fecal pellets, OTHER= particles, DD = diadinoxanthin, DT = diatoxanthin.

Figure 10. A schematic diagram showing phytoplankton and particles (diatom chains, copepods, fecal pellets and aggregates) dynamics in Mausund Bank, Froan archipelago. Brown area indicates the bottom of the bank. The left side of the diagram represents stratified waters from off-bank, with the influence of warm, nutrient-rich Atlantic waters (red) beneath coastal waters (blue). Stratification can suppress nutrients at the surface, which increases the proportion of small (< 20 µm) phytoplankton off-bank. The Atlantic-influenced waters enter at the bank, either through internal waves or similar phenomena, and tidal mixing fuels the growth of microphytoplankton (> 20 µm, including diatom chains). Pico- and nanophytoplankton can feed ciliates or other types of microzooplankton. The high abundance of diatoms stimulates copepod growth, fecal pellet production and aggregate formation on the bank region. High abundance of copepods can serve as food to the upper trophic levels, such as birds and fish, while aggregates can be a source of food for the benthos.

Figure 1

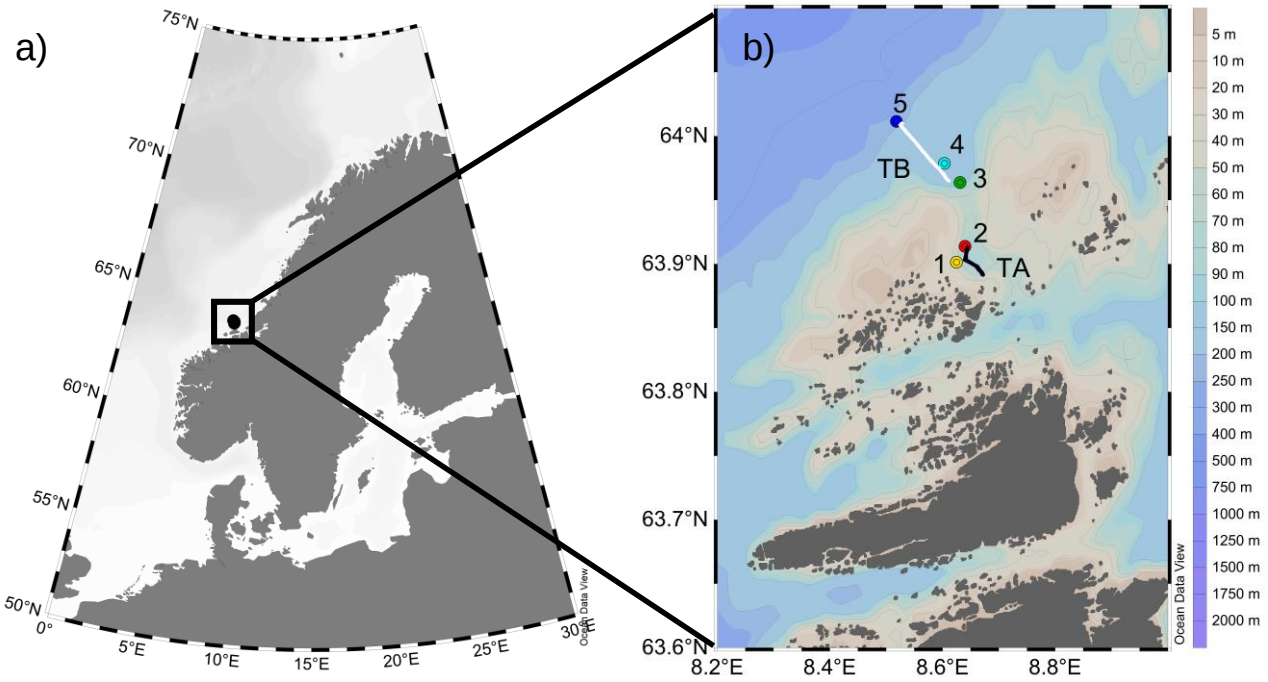
a)
75°N
70°N
65°N
60°N
55°N
50°N
0°
5°E
10°E
15°E
20°E
25°E
30°E
b)
64°N
63.9°N
63.8°N
63.7°N
63.6°N
8.2°E
8.4°E
8.6°E
8.8°E
5
4
3
2
1
TB
TA
5 m
10 m
20 m
30 m
40 m
50 m
60 m
70 m
80 m
90 m
100 m
150 m
200 m
250 m
300 m
400 m
500 m
750 m
1000 m
1250 m
1500 m
1750 m
2000 m
Ocean Data View

Figure 2

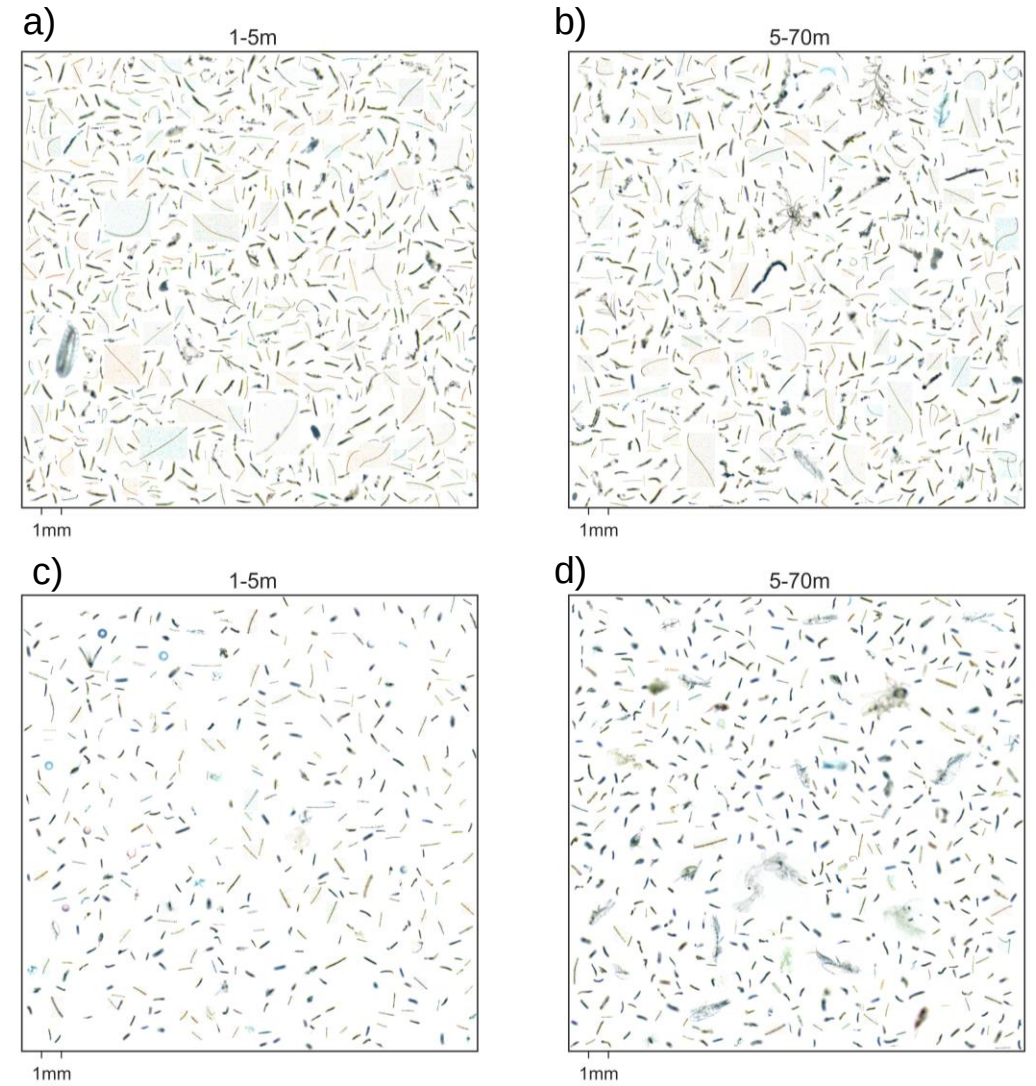

Figure 3

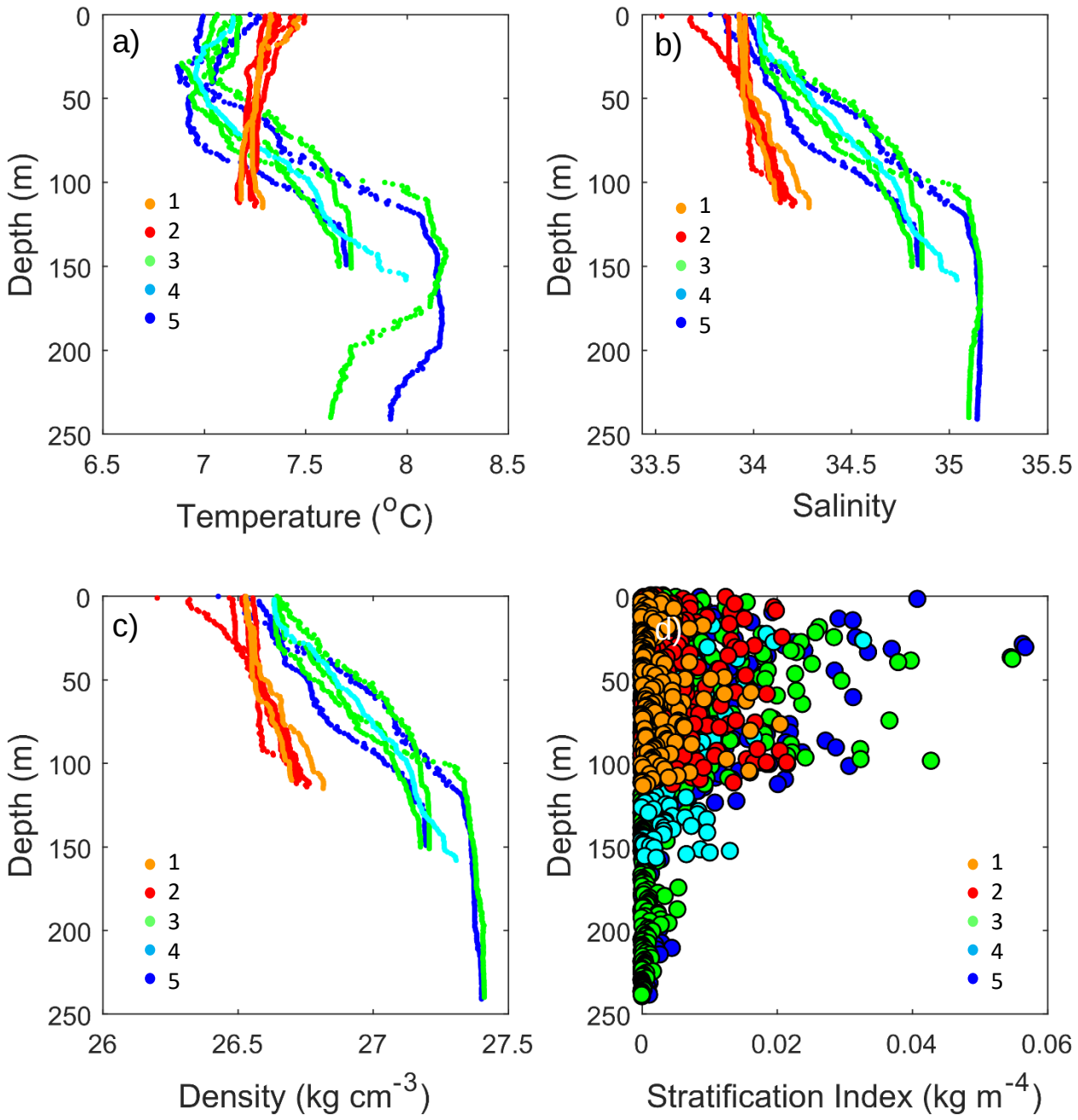
a)
b)
c)
d)
Depth (m)
Temperature (°C)
Salinity
Density (kg cm-3)
Stratification Index (kg m-4)
1
2
3
4
5

Figure 4

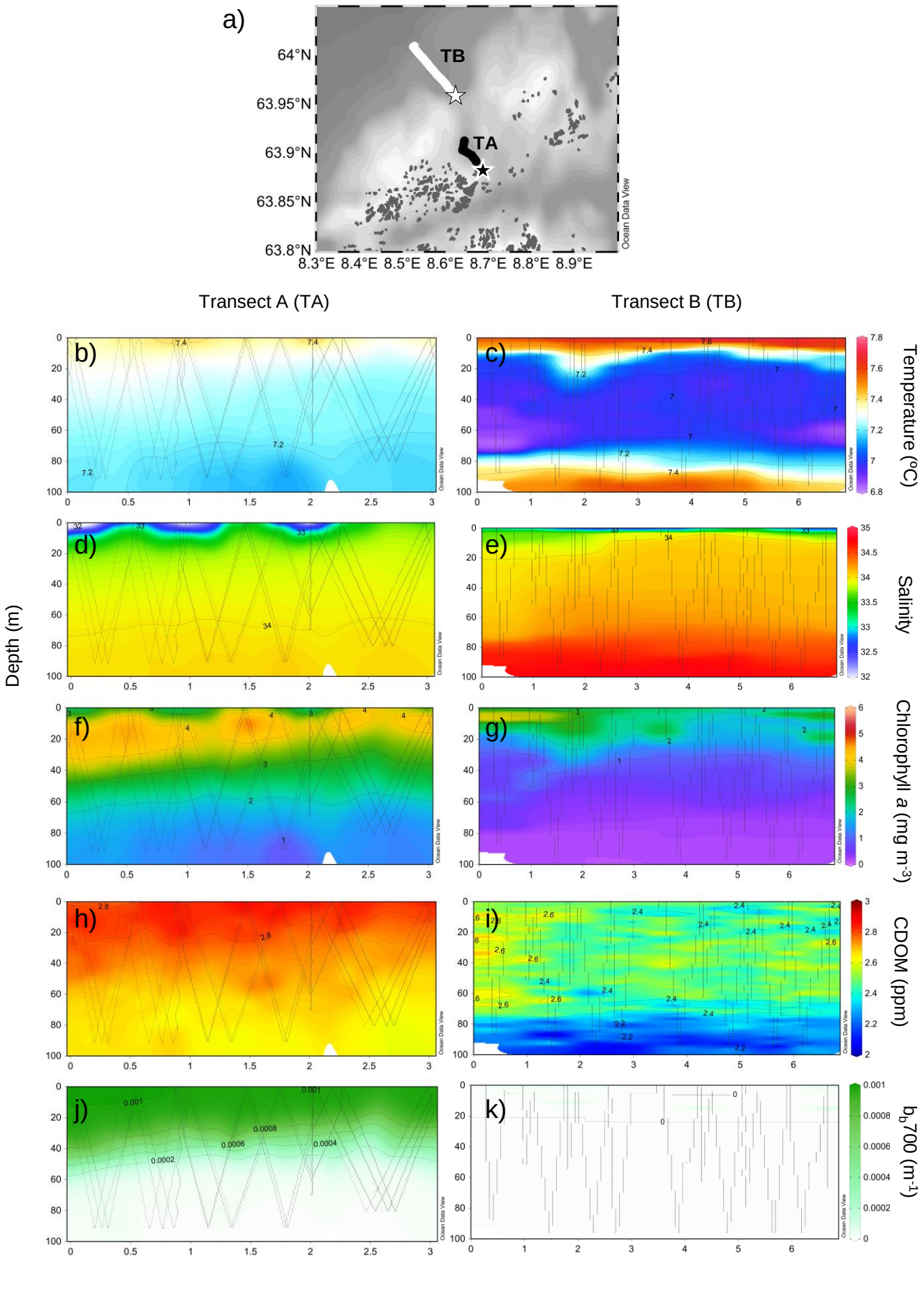
a)
TB
TA
64°N
63.95°N
63.9°N
63.85°N
63.8°N
8.3°E 8.4°E 8.5°E 8.6°E 8.7°E 8.8°E 8.9°E
Ocean Data View
Transect A (TA)
Transect B (TB)
b)
c)
d)
e)
f)
g)
h)
i)
j)
k)
Depth (m)
Temperature (°C)
Salinity
Chlorophyll a (mg m-3)
CDOM (ppm)
bb700 (m-1)
Section distance from star symbol (km)

Figure 5

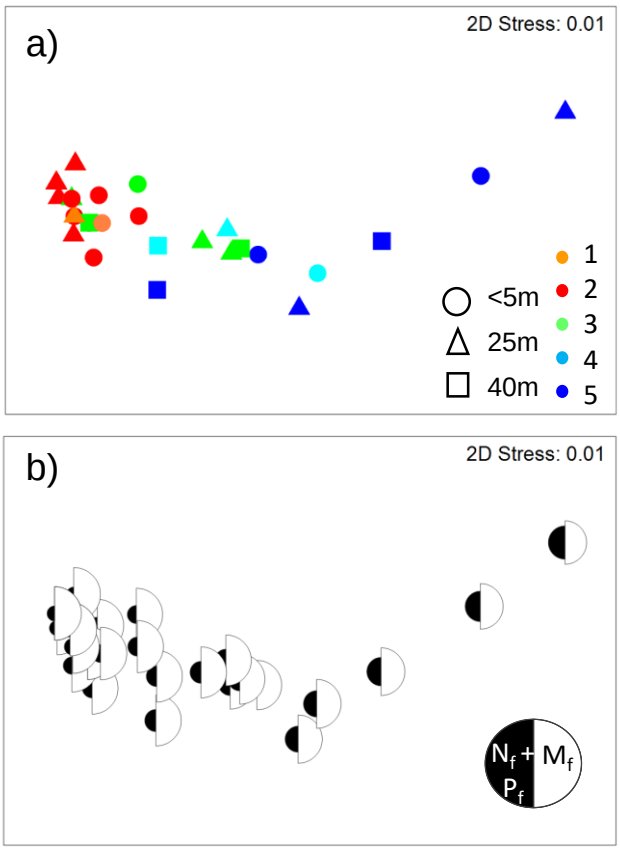

Figure 6

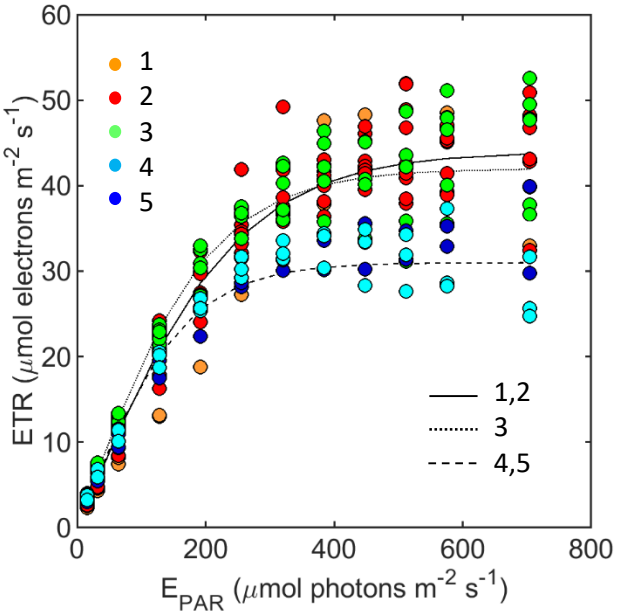
60
50
40
30
20
10
0
0
200
400
600
800
ETR (μmol electrons m^{-2} s^{-1})
E_{PAR} (μmol photons m^{-2} s^{-1})
1
2
3
4
5
1,2
3
4,5

Figure 7

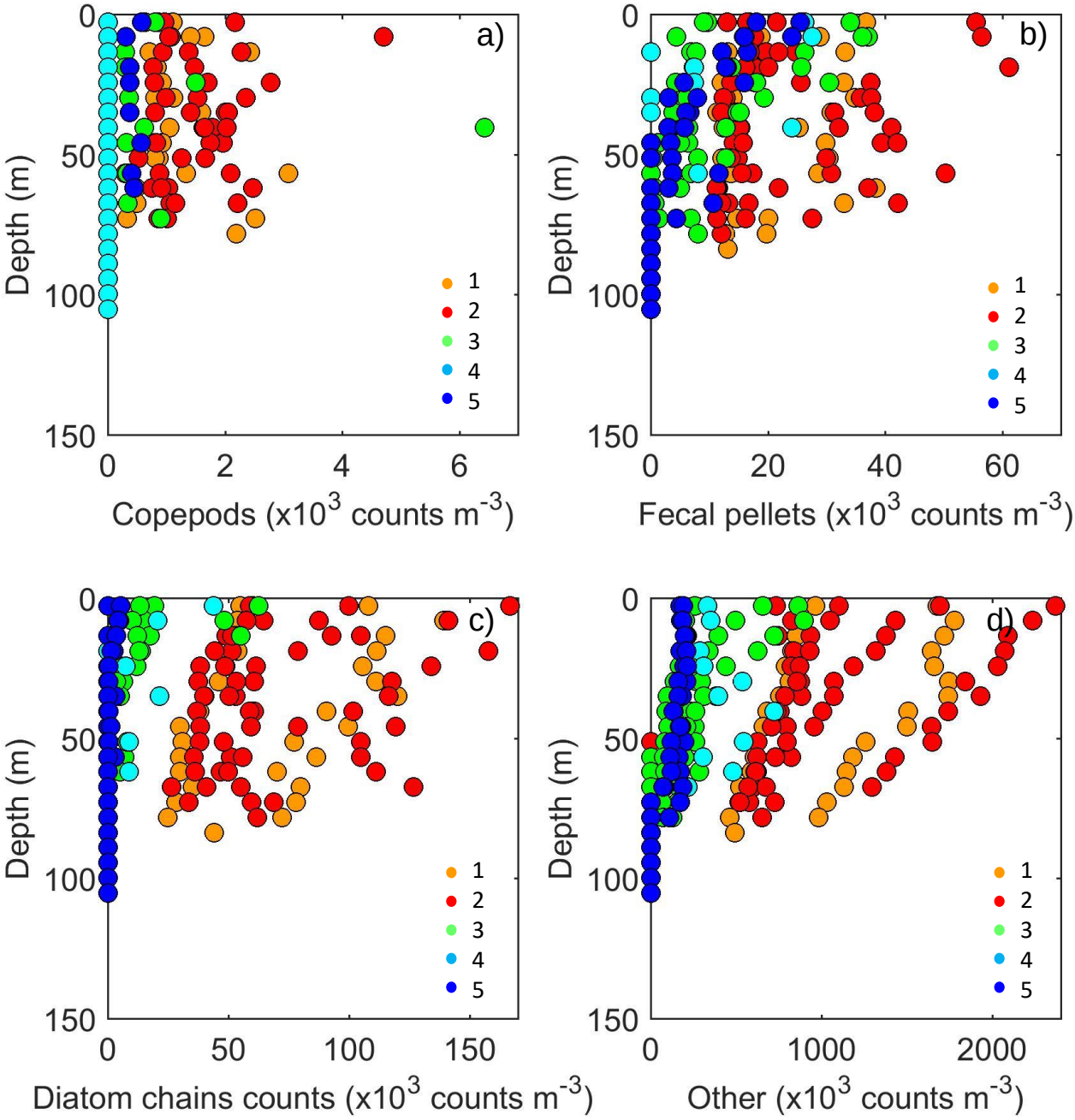
a)
b)
c)
d)
Depth (m)
0
50
100
150
1
2
3
4
5
Copepods (x10^3 counts m^-3)
0
2
4
6
Fecal pellets (x10^3 counts m^-3)
0
20
40
60
Diatom chains counts (x10^3 counts m^-3)
0
50
100
150
Other (x10^3 counts m^-3)
0
1000
2000

Figure 8

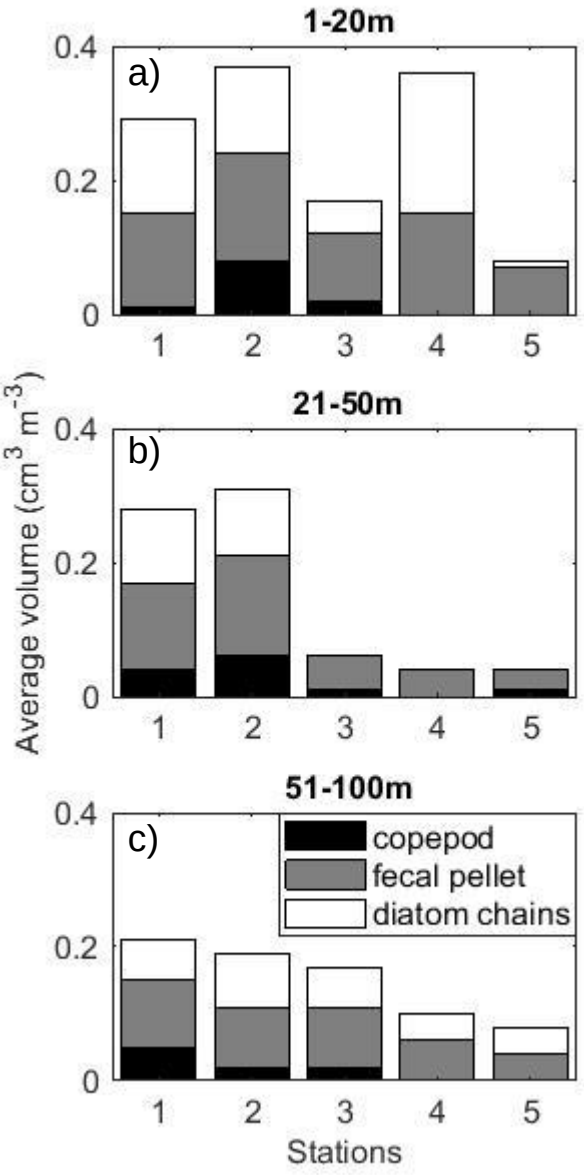
1-20m
a)
0.4
0.2
0
1
2
3
4
5
21-50m
b)
0.4
0.2
0
1
2
3
4
5
51-100m
c)
0.4
0.2
0
1
2
3
4
5
Stations
copepod
fecal pellet
diatom chains
Average volume (cm3 m-3)

Figure 9

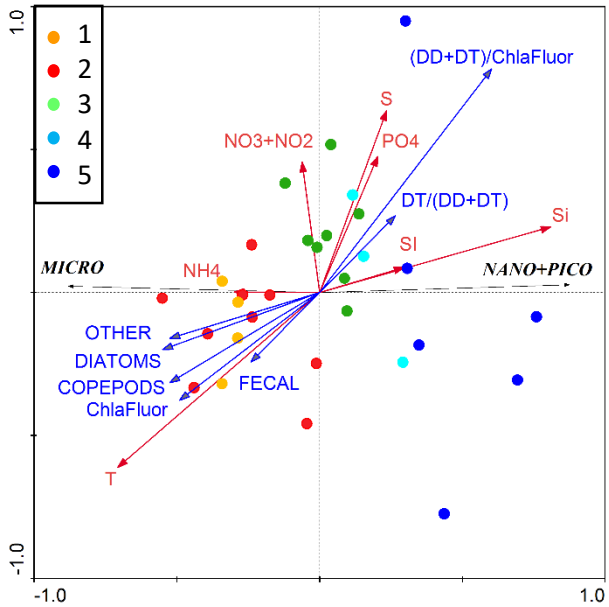
1
2
3
4
5
1.0
-1.0
-1.0
1.0
(DD+DT)/ChlaFluor
S
NO3+NO2
PO4
DT/(DD+DT)
Si
SI
MICRO
NANO+PICO
NH4
OTHER
DIATOMS
COPEPODS
ChlaFluor
FECAL
T

Figure 10

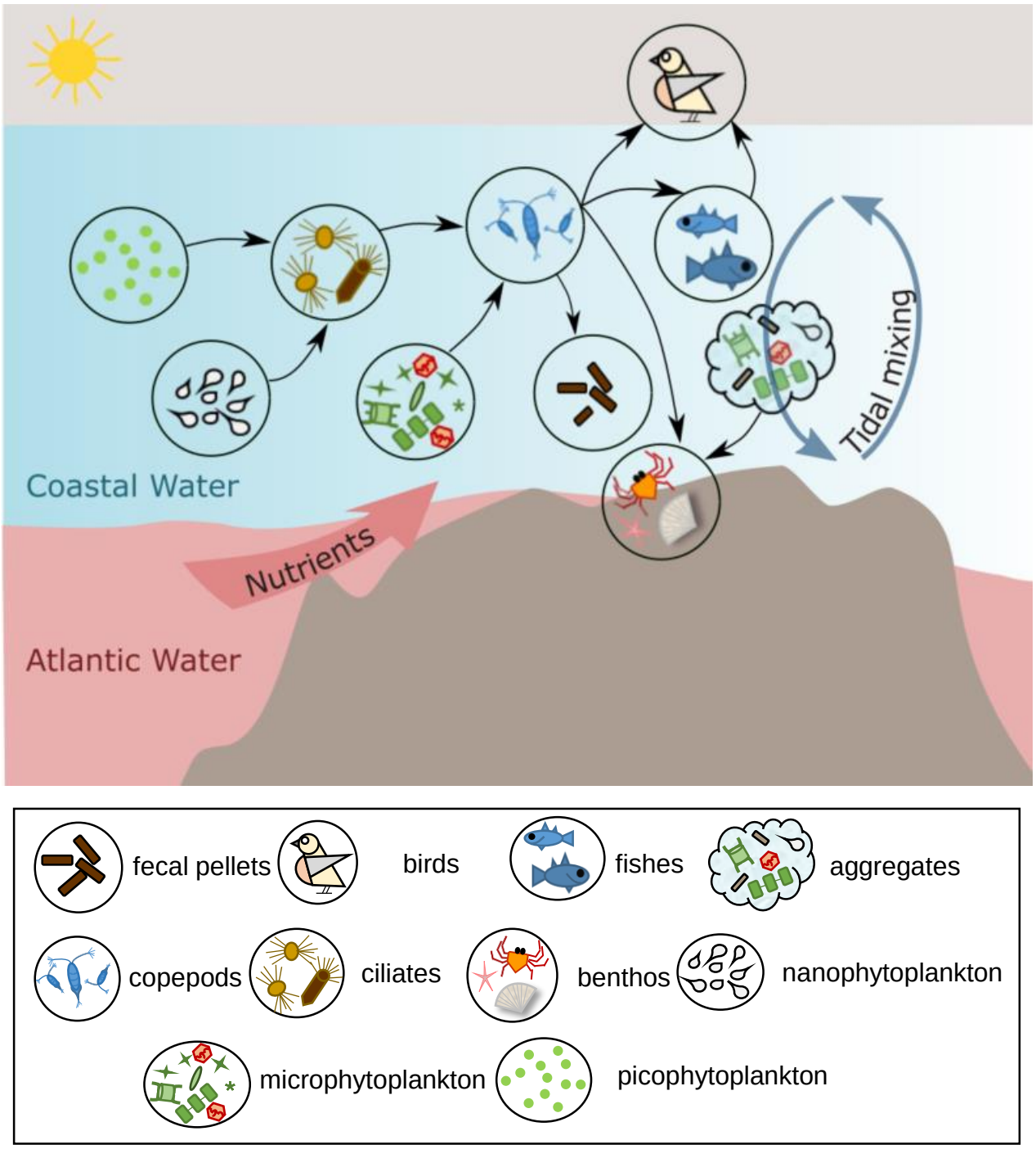
Coastal Water
Nutrients
Atlantic Water
Tidal mixing
fecal pellets
birds
fishes
aggregates
copepods
ciliates
benthos
nanophytoplankton
microphytoplankton
picophytoplankton

Table 1. Date, time (GMT), CTD cast number, bottom depth (m) and tidal condition at each of the five stations revisited.

Day	Time	Station	CTD Cast	Bottom depth (m)	Tide
08.05.2017	15:40	2	1	119	ebb
09.05.2017	10:35	5	2	250	high
09.05.2017	14:20	3	3	150	ebb
09.05.2017	16:30	2	4	120	low
09.05.2017	18:28	1	5	125	low
10.05.2017	11:00	5	6	250	high
10.05.2017	13:26	4	7	168	high
10.05.2017	15:30	3	8	156	ebb
10.05.2017	16:45	2	9	115	low
10.05.2017	18:17	1	10	124	low
11.05.2017	09:15	3	11	170	rise
11.05.2017	11:00	2	12	120	high
11.05.2017	15:30	1	13	123	ebb
11.05.2017	17:25	2	14	120	low

Table 2. Average and standard deviations of biological and environmental parameters of each station. NO_3+NO_2 = nitrate and nitrite; PO_4 = phosphate; $Si(OH)_4$ = silicate; NH_4 = ammonium; Chla_{Fluor} = fluorometric-derived chlorophyll *a*, DD = diadinoxanthin, DT = diatoxanthin.

	Station 1 n=4	Station 2 n=9	Station 3 n=8	Station 4 n=3	Station 5 n=6
Microphytoplankton (%)	91 ± 1	91 ± 2	87 ± 4	82 ± 5	73 ± 8
Nano- + picophytoplankton (%)	9 ± 2	9 ± 2	13 ± 4	18 ± 5	25 ± 8
NH_4 (µM)	0.6 ± 0.1	0.5 ± 0.3	0.4 ± 0.1	0.6 ± 0.3	0.4 ± 0.2
PO_4 (µM)	0.1 ± 0.1	0.1 ± 0	0.1 ± 0	0.1 ± 0.1	0.1 ± 0
NO_3+NO_2 (µM)	2.0 ± 0.3	2.4 ± 0.5	2.2 ± 0.6	1.5 ± 0.9	1.9 ± 0.3
$Si(OH)_4$ (µM)	0.4 ± 0	0.5 ± 0.1	1.0 ± 0.3	1.3 ± 0.2	1.8 ± 0.1
Chlorophyll *a* (mg Chla_{Fluor} m^{-3})	4.0 ± 0.3	4.2 ± 1.1	2.8 ± 0.9	2.1 ± 1.9	1.9 ± 1.1
Temperature (ºC)	7.3 ± 0.1	7.3 ± 0.1	7.1 ± 0.1	7.0 ± 0.1	7.0 ± 0.1
Salinity	33.9 ± 0	33.9 ± 0	34.1 ± 0.1	34.1 ± 0.1	34.0 ± 0.1
Stratification Index × 10^{-3} (kg m^{-4})	2 ± 1	5 ± 7	14 ± 14	4 ± 4	11 ± 11
Copepods (× 10^3 counts m^{-3})	1.0 ± 0.4	1.2 ± 0.5	0.2 ± 0.3	0 ± 0	0.1 ± 0.2
Fecal pellets (× 10^3 counts m^{-3})	23 ± 10	26 ± 14	14 ± 10	10 ± 7	11 ± 7
Diatom chains (× 10^3 counts m^{-3})	83 ± 37	83 ± 40	13 ± 18	10 ± 10	2 ± 1
Other particles (× 10^3 counts m^{-3})	1275 ± 496	1381 ± 546	359 ± 235	369 ± 67	181 ± 16
(DD+DT)/ Chla_{Fluor} (w:w)	0.1 ± 0.1	0.1 ± 0.1	0.1 ± 0	0.3 ± 0.1	0.2 ± 0.1
DT/(DD+DT) (w:w)	0.2 ± 0	0.2 ± 0	0.2 ± 0.1	0.3 ± 0	0.3 ± 0.1

Table 3. Average, standard deviation and number of observations (*n*) of photophysiological parameters (maximum electron transport rate (ETR_{max}), initial slope of the curve (α) and onset saturation irradiance (E_k)) and goodness-of-fit ((the sum of squares due to error, SSE), R^2 and root mean squared error (RMSE)) of curves for each station. Units of photophysiological parameters are: ETR_{max}, µmol electrons m^{-2} s^{-1}; α, electrons /photons; E_k (ETR_{max}/α), µmol photons m^{-2} s^{-1}. Values from each curve are shown in Table S2 (supplementary material).

Station	*n*	ETR_{max}	α	E_k	SSE	R^2	RMSE
1	3	48 ± 4	0.154 ± 0.030	311 ± 33	53 ± 31	0.98 ± 0.01	2.2 ± 0.8
2	8	49 ± 2	0.167 ± 0.024	292 ± 38	76 ± 34	0.97 ± 0.01	2.6 ± 0.6
3	4	49 ± 5	0.184 ± 0.016	265 ± 47	102 ± 64	0.96 ± 0.03	2.9 ± 1.1
4	2	35 ± 2	0.160 ± 0.018	218 ± 38	22 ± 1	0.98 ± 0	1.4 ± 0
5	4	36 ± 5	0.191 ± 0.024	190 ± 30	57 ± 39	0.96 ± 0.03	2.2 ± 0.7

Table 4. Variance of each explanatory (environmental) variable (temperature (°C), nitrate and nitrite (NO_3+NO_2), phosphate (PO_4), silicate ($Si(OH)_4$) and ammonium (NH_4) (μM), salinity and stratification index (SI) analyzed alone (λ_1, marginal effects) or with other forward-selected variables (λa, conditional effects). Significant *p-values* (**p < 0.001 and *p < 0.05) represent the variables that significantly explain the variation in the analysis.

Marginal Effects					Conditional	Effects		
Variable	λ1				Variable	λ*a*	*P*	*F*
$Si(OH)_4$	0.51				$Si(OH)_4$	0.51	0.001**	28.6
Temperature	0.39				NO_3+NO_2	0.18	0.001**	16.0
NH_4	0.07				NH_4	0.06	0.025*	6.0
SI	0.07				Salinity	0.01	0.260	1.4
Salinity	0.04				Temperature	0.01	0.507	0.6
NO_3+NO_2	0.03				SI	0	0.521	0.4
PO_4	0				PO_4	0	0.792	0.1
Axes	1	2	3	4	Total variance			
Eigen-values	0.771	0.001	0.227	0.001	1			
Phytoplankton group-environment correlations	0.879	0.612	0.000	0.000				
Cumulative percentage variance								
of group data	77.1%	71.2%	99.9%	100.0%				
of group-environment relation	99.9%	100.0%	0.0%	0.0%				
Sum of all eigenvalues					1			
Sum of all canonical eigenvalues					0.731			

Table S1. List of taxa observed from samples collected from distinct regions (A and B), dates (8^{th} to 11^{th} May) and stations (1-5). Black areas indicate taxa presence in the sample.

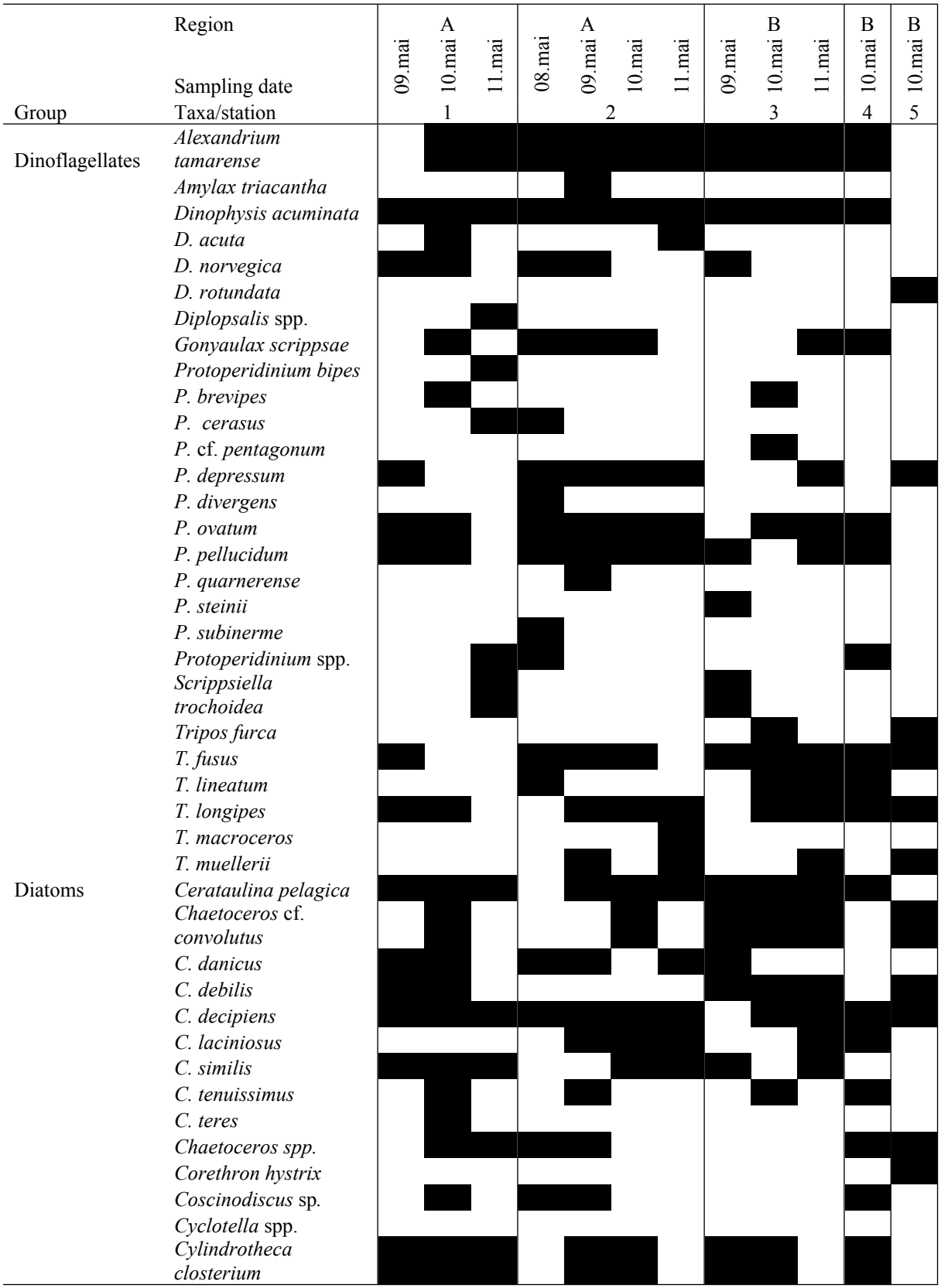

Table S1 (continuation). List of taxa observed from samples collected from distinct regions (A and B), dates (8th to 11th May) and stations (1-5). Black areas indicate taxa presence.

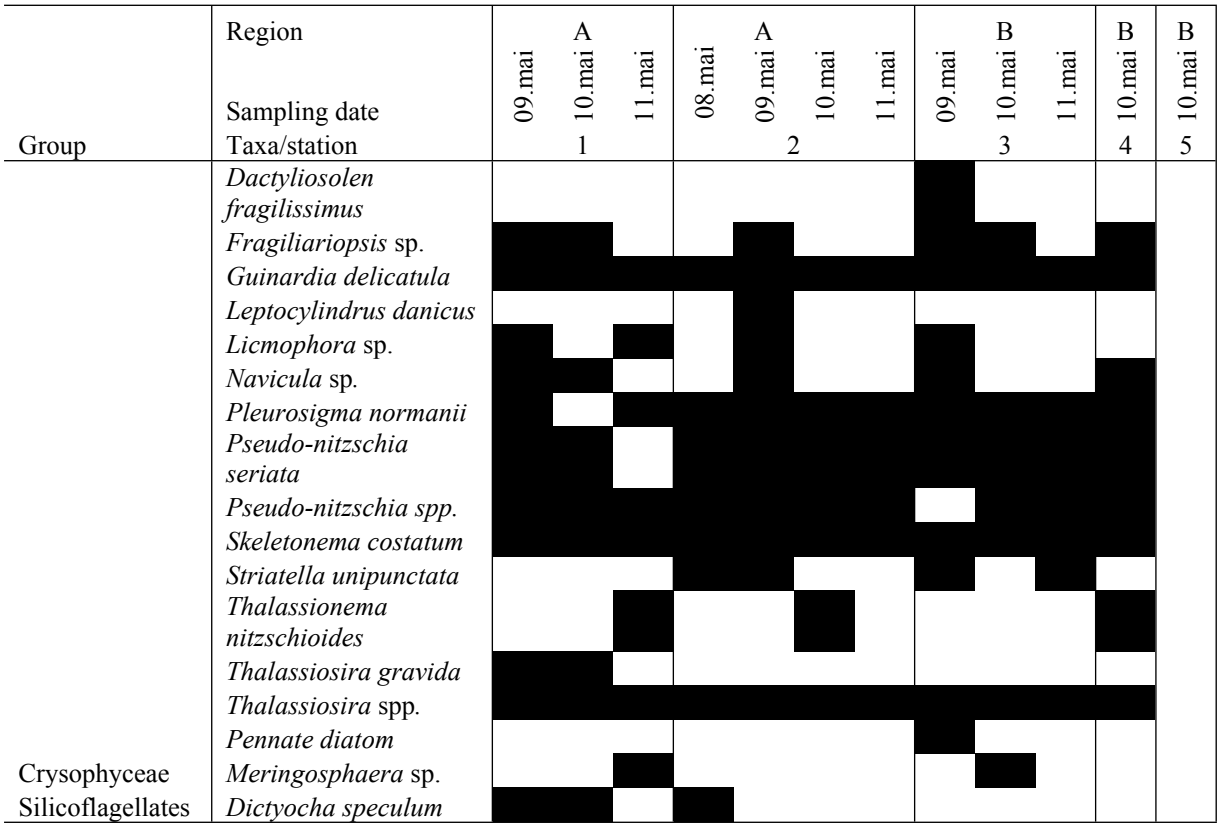

Table S2. Photophysiological parameters (maximum electron transport rate (ETR_{max}), initial slope of the curve (α) and onset saturation irradiance (E_k)) and goodness-of-fit (the sum of squares due to error (SSE), degrees of freedom (DOF), R^2 and root mean squared error (RMSE)) of each curve measured on distinct stations, CTD casts and depths. Units of photophysiological parameters are: ETR_{max}, µmol electrons m^{-2} s^{-1}; α, electrons/photons; E_k, µmol photons m^{-2} s^{-1}. Values from each curve are shown in Table S2 (supplementary material).

Station	Depth	CTD cast	ETR_{max}	α	E_k	SSE	DOF	R^2	RMSE
1	1	10	44	0.1357	326	79	10	0.97	2.8
1	25	10	46	0.1381	334	63	10	0.98	2.5
1	25	13	52	0.1888	274	19	11	0.99	1.4
2	1	4	46	0.1517	306	79	11	0.97	2.7
2	3	9	45	0.1481	307	42	11	0.99	2.0
2	3	12	49	0.2157	227	97	11	0.97	3.0
2	3	14	50	0.1405	354	142	11	0.94	3.6
2	25	4	47	0.1793	261	37	11	0.99	1.8
2	25	9	48	0.157	308	73	11	0.98	2.6
2	25	12	52	0.1772	291	50	11	0.98	2.1
2	25	14	47	0.1666	280	86	10	0.96	2.9
3	3	11	49	0.1783	273	177	11	0.94	4.0
3	25	3	51	0.195	260	22	11	0.99	1.4
3	25	8	52	0.1634	320	95	11	0.97	2.9
3	25	11	41	0.1986	206	112	11	0.94	3.2
4	3	7	36	0.1467	245	23	11	0.99	1.4
4	25	7	33	0.1728	191	22	11	0.98	1.4
5	1	2	34	0.1948	175	106	11	0.92	3.1
5	3	6	37	0.1601	231	33	11	0.98	1.7
5	25	2	31	0.1918	162	67	11	0.93	2.5
5	25	6	42	0.2191	192	20	8	0.99	1.6